Collective many-body resonances in condensed phase nonlinear spectroscopy

Andreas Tortschanoff and Shaul Mukamel
Department of Chemistry, University of Rochester, Rochester, New York 14627-0216

(Received 31 July 2001; accepted 23 October 2001)

The optical response of assemblies of electronic and vibrational chromphores may show two types of collective resonances induced by either direct short-range coupling (multiple quantum coherence) or by long-range macroscopic local field and cascading processes. Using a unified approach for both types of resonances, we demonstrate how specific signatures in line shapes, phase profiles, and density dependence may be used to distinguish between the two. New high harmonic resonances at combinations and multiples of optical frequencies of the single exciton transitions are predicted in the $\mathbf{k}_1+\mathbf{k}_2-\mathbf{k}_3$ four wave mixing signal for several model systems. © *2002 American Institute of Physics.* [DOI: 10.1063/1.1427721]

I. INTRODUCTION

The nonlinear optical response of systems with high density of chromophores depends on the fact that each chromophore is driven by an external local field $\tilde{E}_l$ which is different from the average (Maxwell) field E. This gives rise to macroscopic *local field* and *cascading* contributions[1,2] that can induce new resonances and other interesting collective many-body effects that need to be accounted for in the interpretation of multidimensional spectroscopies.[3–5] Chromophores with nonoverlapping charge distributions couple in two ways:[6] short-range microscopic interactions depend on the *longitudinal* electric field and may be described by replacing the chromophore eigenstates by those of aggregates. Long-range coupling occurs via the *transverse* electric field which is generated by one group of chromophores and interacts with the others. These interactions can be described by the mean-(local-) field approach,[1,7,8] where the effects of interparticle interactions are incorporated through an effective local field which is related to the external Maxwell field by the Lorentz Formula.[2] This implies that the coherent polarization generated within the sample adds to the electric field and creates new interactions. The mean-field approximation is justified for the long-range interactions where microscopic details are averaged out. Such details are included in the short-range direct interactions. Combining both contributions provides a rigorous description of the optical response.

The connection between macroscopic susceptibilities and microscopic polarizabilities is crucial for comparing computed polarizabilities with condensed phase measurements and has drawn considerable attention since the early days of nonlinear optics. In the simplest approach, the Clausius Mossotti expression for the dielectric function based on the local-field formulation of the linear response[9] has been extended to the nonlinear response.[2] This level of theory has been primarily used to compare computed frequency-domain off resonant polarizabilities with bulk measurements, and is commonly used for the design of optical materials. This theory has been extended to the time domain using equations of motion for a single molecule driven by the local field.[8] The limitations of the local-field approximation for modeling resonant techniques were pointed out and a unified treatment of nonlinear signals that goes beyond the local-field approximation, and includes genuine many-body effects, was subsequently obtained using the nonlinear exciton equations of motion (NEE),[10–12] which include additional dynamic variables involving few molecules. The local field approximation is then recovered as the lowest order in a systematic hierarchy when all dynamical variables are factorized into products of single molecule variables.

Coherent femtosecond measurements provide a direct probe for resonant transitions of coupled electronic and vibrational chromophores.[1,3,4,13–19] Signatures of local field and cascading were found in femtosecond four wave mixing signals in GaAs quantum wells[20–22] and in the gas phase,[23–25] femtosecond fifth order Raman measurements in molecular liquids[26,27] and enhanced magnitudes of off resonant polarizabilities.[10,11,28]

In this paper we provide a unified treatment of the signatures of *both* types of coupling in the third order nonlinear response.[29] We predict and analyze new high harmonic resonances originating from destroying the time ordering of the incident fields by the local field which were found in NMR[30,31] and should be directly observed optically.

Third order time-resolved nonlinear spectroscopy offers a variety of different techniques characterized by their pulse-sequence, wave-vector geometry and pulse frequencies.[1,5] In a four wave mixing experiment, three electric fields interact with the system and generate a polarization (and a signal) in the directions $\mathbf{k}_s=\pm\mathbf{k}_1\pm\mathbf{k}_2\pm\mathbf{k}_3$.[12] To clarify the origin of different kinds of many-body resonances, we will concentrate on one technique, the reverse photon echo (RPE) with $\mathbf{k}_s=\mathbf{k}_1+\mathbf{k}_2-\mathbf{k}_3$, where the first two pulses ($\mathbf{k}_1$ and $\mathbf{k}_2$) are time coincident. However, similar effects will show up in other four wave mixing techniques and can be treated using the present approach. The RPE technique is realized if the photon echo pulse sequence is reversed in time (hence its

name). We focus on the RPE since for independent two-level systems at low density the RPE signal vanishes;[7,21,22] the signal thus results exclusively from many-body effects, either short or long range, making this technique especially sensitive and particularly suitable for the observation of collective resonances.

II. LOCAL FIELD AND CASCADING EFFECTS IN THE NONLINEAR RESPONSE

The heterodyne signal in nonlinear spectroscopy is proportional to the induced polarization which in turn can be expanded perturbatively in the average electric field. The nth order nonlinear polarization $P^{(n)}$ is:[1]

$$P^{(n)}(\mathbf{r},\tau_c)=\int_{-\infty}^{\tau_c}d\tau_n\int_{-\infty}^{\tau_n}d\tau_{n-1}\ldots\int_{-\infty}^{\tau_2}d\tau_1 \times R^{(n)}(\tau_n;\tau_{n-1},\ldots,\tau_1) \times E(\mathbf{r},\tau_n)E(\mathbf{r},\tau_{n-1})\ldots E(\mathbf{r},\tau_1) \quad (1)$$

Here the Maxwell field $E(\mathbf{r},\tau)$ is the average transverse electric field which interacts with the system under investigation at times $\tau=\tau_1,\ldots\tau_n$ and τ_c is the observation time. The nth order response function $R^{(n)}$ is given by the sum of all possible Liouville-space pathways. Due to its time-ordered (causal) structure, $R^{(n)}$ is nonzero only for $\tau_1<\tau_2<\ldots<\tau_n$.

The local-field approximation (LFA) provides a simple way to relate the microscopic polarizabilities of isolated molecules to the macroscopic susceptibilities.[1,8,10,11,28] At this level of theory the response of an ensemble of particles is reduced to that of a single particle interacting with a local field. In the long wavelength limit the local field $\widetilde{E}_l$ is related to the external field E by the Lorentz formula[2,9,29]

$$\widetilde{E}_l(t)=E(t)+\frac{4\pi}{3}P(t), \quad (2)$$

where $P(t)$ is the polarization per unit volume. The polarization of a single chromophore (i.e., a single molecule or an aggregate of coupled molecules) can be expanded in terms of its response functions (polarizabilities) α, β, $\gamma,\ldots$ to various orders in the local field, and the total nonlinear polarization per unit volume of a macroscopic sample is

$$P^{NL}(\mathbf{r},\tau_c)=\rho_0\int_{-\infty}^{\tau_c}d\tau_3\int_{-\infty}^{\tau_3}d\tau_2\int_{-\infty}^{\tau_2}d\tau_1 s(\tau_c-\tau_3) \times\beta(\tau_3,\tau_2,\tau_1)\widetilde{E}_l(\mathbf{r},\tau_2)\widetilde{E}_l(\mathbf{r},\tau_1) +\rho_0\int_{-\infty}^{\tau_c}d\tau_4\int_{-\infty}^{\tau_4}d\tau_3\int_{-\infty}^{\tau_3}d\tau_2\int_{-\infty}^{\tau_2}d\tau_1 \times s(\tau_c-\tau_4)\gamma(\tau_3,\tau_2,\tau_1)\widetilde{E}_l(\mathbf{r},\tau_2)\widetilde{E}_l(\mathbf{r},\tau_1)+\ldots, \quad (3)$$

where $P\equiv P^{(1)}+P^{NL}$ and ρ_0 is the molecular number density.

Both the total polarization P and the local field $\widetilde{E}_l$ can be expanded perturbatively in powers of the Maxwell field E, and we denote the jth order terms by $P^{(j)}$ and $\widetilde{E}_l^{(j)}$, respectively. The expansion of the local field is obtained by substituting the expansion of P in Eq. (2). The linear part of the local field $E_l\equiv\widetilde{E}_l^{(1)}$ is connected to the Maxwell field E by the Clausius Mossotti relation:

$$E_l(\mathbf{r},t)\equiv\widetilde{E}_l^{(1)}(\mathbf{r},t)=\int_{-\infty}^{t}s(t-\tau)E(\mathbf{r},\tau)d\tau, \quad (4)$$

where,[32]

$$s(\omega)=\frac{1}{1-(4\pi)/3\,\rho_0\alpha(\omega)}. \quad (5)$$

The symbol α is the linear response function (polarizability) of a single aggregate:

$$\alpha(t)=i\theta(t)\sum_{e''}\mu_{e''g}^2\exp[(-i\varepsilon_{e''g}-\Gamma_{eg})t]-\text{c.c.}, \quad (6)$$

where g denotes the ground state and the sum runs over all one-exciton states $|e''\rangle$ in the system. Plugging Eq. (4) in Eq. (2) we obtain

$$\widetilde{E}_l(\mathbf{r},\tau)=\int_{-\infty}^{\tau}d\tau' s(\tau-\tau')E(\mathbf{r},\tau') +\frac{4\pi}{3}\int_{-\infty}^{\tau}d\tau' s(\tau-\tau')P^{NL}(\mathbf{r},\tau'). \quad (7)$$

The first term in the r.h.s. of Eq. (7), which corresponds to the first order term E_l is responsible for *local* field effects, while the second term describes effects of the nonlinear polarization that generate *cascading* contributions. Substitution of Eq. (7) in Eq. (3) yields an integral equation for the nonlinear polarization P^{NL}. An iterative solution of this equation results in the expansion of P^{NL} in powers of the Maxwell field E. Using these relations, we can thus express the polarization order by order in the Maxwell field.

The linear polarization is given by

$$P^{(1)}(\mathbf{r},\tau_c)=\rho_0\int_{-\infty}^{\tau_c}d\tau_2\int_{-\infty}^{\tau_2}d\tau_1 \times\alpha(\tau_c,\tau_2)s(\tau_2-\tau_1)E(\mathbf{r},\tau_1). \quad (8)$$

The second order polarization has no cascading contributions and the many-body corrections enter solely through the linear first term of $\widetilde{E}_l$

$$P^{(2)}(\mathbf{r},\tau_c)=\rho_0\int_{-\infty}^{\tau_c}d\tau_3\int_{-\infty}^{\tau_3}d\tau_2\int_{-\infty}^{\tau_2}d\tau_1 s(\tau_c-\tau_3) \times\beta(\tau_3,\tau_2,\tau_1)E_l(\mathbf{r},\tau_2)E_l(\mathbf{r},\tau_1). \quad (9)$$

For the third order polarization, which is the focus of this article we need to calculate $\widetilde{E}_l^{(2)}$ in addition to E_l by substituting Eq. (3) into Eq. (7) and making use of Eq. (2). We then get

$$P^{(3)}(\mathbf{r},\tau_c)=\rho_0\int_{-\infty}^{\tau_c}d\tau_4\int_{-\infty}^{\tau_4}d\tau_3\int_{-\infty}^{\tau_3}d\tau_2\int_{-\infty}^{\tau_2}d\tau_1 s(t-\tau_4)\gamma(\tau_4,\tau_3,\tau_2,\tau_1)E_l(\mathbf{r},\tau_1)E_l(\mathbf{r},\tau_2)E_l(\mathbf{r},\tau_3)$$
$$+\rho_0\int_{-\infty}^{\tau_c}d\tau_3\int_{-\infty}^{\tau_3}d\tau_2\int_{-\infty}^{\tau_2}d\tau_1 s(t-\tau_3)\beta(\tau_3,\tau_2,\tau_1)[\tilde{E}_l^{(2)}(\mathbf{r},\tau_2)E_l(\mathbf{r},\tau_1)+E_l(\mathbf{r},\tau_2)\tilde{E}_l^{(2)}(\mathbf{r},\tau_1)], \quad (10)$$

where

$$\tilde{E}_l^{(2)}(\mathbf{r},\tau)=\frac{4\pi\rho_0}{3}\int_{-\infty}^{\tau}d\tau'\int_{-\infty}^{\tau'}d\tau_3\int_{-\infty}^{\tau_3}d\tau_2\int_{-\infty}^{\tau_2}d\tau_1 \times s(\tau-\tau')s(\tau'-\tau_3)\beta(\tau_3,\tau_2,\tau_1)E_l(\mathbf{r},\tau_2)E_l(\mathbf{r},\tau_1). \quad (11)$$

For completeness we also present the corresponding frequency domain expressions for the first, second, and third order susceptibilities ($\chi^{(1)}$, $\chi^{(2)}$, and $\chi^{(3)}$, respectively) obtained by the Fourier transform of the above expressions[1]

$$\chi^{(1)}(-\omega;\omega)=\rho_0\alpha(\omega)s(\omega), \quad (12)$$

$$\chi^{(2)}(-\omega_s;\omega_1,\omega_2)=\rho_0\beta(\omega_1,\omega_2)s(\omega_1)s(\omega_2)s(\omega_s), \quad (13)$$

and

$$\chi^{(3)}(-\omega_s;\omega_1,\omega_2,\omega_3)=\rho_0\gamma(\omega_1,\omega_2,\omega_3)s(\omega_1)s(\omega_2)s(\omega_3)s(\omega_s)+\frac{2\pi}{3}\rho_0^2 s(\omega_1)s(\omega_2)s(\omega_3)s(\omega_s)\times\sum_{\text{perm}}\beta(\omega_1,\omega_2+\omega_3)\beta(\omega_2,\omega_3)s(\omega_2+\omega_3), \quad (14)$$

where perm stands for the sum over all permutations of the frequencies of the electric fields ω_1, ω_2, and ω_3. $\omega_s=\omega_1+\omega_2+\omega_3$ is the signal field frequency (different signals with all possible choices of sign in $\omega_s=\pm\omega_1\pm\omega_2\pm\omega_3$ are given by simply changing the signs of various frequencies).

III. THE REVERSE PHOTON ECHO IN AGGREGATES WITHOUT LOCAL-FIELD EFFECTS

In this paper we will focus on local-field effects and only take into account the linear (free induction decay) contributions to Eq. (7). Higher-order (cascading) processes coming from the second term in Eq. (7),[1,8] which are interesting on their own and were observed experimentally,[26,27,33–35] will not be considered here. By neglecting the second term in Eq. (7), we obtain for the third order polarization,[29]

$$P^{(3)}(\mathbf{r},\tau_c)=\int_{-\infty}^{\tau_c}d\tau_4\int_{-\infty}^{\tau_c}d\tau_3\int_{-\infty}^{\tau_3}d\tau_2\int_{-\infty}^{\tau_2}d\tau_1 s(\tau_c-\tau_4)\times R^{(3)}(\tau_4,\tau_3,\tau_2,\tau_1)E_l(\mathbf{r},\tau_3)E_l(\mathbf{r},\tau_2)E_l(\mathbf{r},\tau_1). \quad (15)$$

Note that in Eq. (15) we use the sample response function $R^{(3)}$ and not the molecular polarizability γ. This allows one to include local interactions directly into the response function. However for a system of noninteracting molecules, $R^{(3)}$ is related to the molecular polarizabilities simply by $R^{(3)}=\rho_0\gamma$.

To establish a reference for discussing local-field effects, we shall summarize in this section what should be expected in their absence. We then set $E(\mathbf{r},\tau_c)$ in Eq. (1) to be the external electric field, which is directly controlled experimentally. The RPE experiment involves a sequence of two pulses a,b peaking at times τ_a, τ_b and described by their (complex) field amplitudes E_a, E_b, frequencies ω_a, ω_b and wave vectors $\mathbf{k}_a$, $\mathbf{k}_b$. The pulses are assumed to be impulsive, i.e., very short compared to all relevant time scales (except for the optical period) and are given by:

$$E(\mathbf{r},t)=E^a(\mathbf{r},t)+E^b(\mathbf{r},t)+\text{c.c.}, \quad (16)$$

where c.c. denotes the complex conjugate and

$$E^j(\mathbf{r},t)\equiv e^{i\mathbf{k_j r}}E^j(t)=E_j\delta(t-\tau_j)e^{i\mathbf{k_j r}}e^{-i\omega_j(t-\tau_j)},\quad j=a,b. \quad (17)$$

We assume that pulse a arrives first ($\tau_a<\tau_b$) and denote the delay between the pulses by t_{ba}, and the time between the second pulse and the detection by t_{cb} ($t_{cb}\equiv\tau_c-\tau_b$, $t_{ba}\equiv\tau_b-\tau_a$) (see Fig. 1). Note that the amplitudes E_a and E_b are complex. The complex fields provide a convenient bookkeeping of the phase. These pulses are defined in the "envelope delayed form"[12,31,36] as generated by an interferometer pathlength difference. All electric field parameters (labeled with the subscripts a,b), and in particular the time delays t_{ba}, t_{cb}, can be controlled in the experiment. This is in contrast to the microscopic interaction times τ_1, τ_2, τ_3 in Eq. (15) which need to be integrated out.

The level scheme displayed in the inset of Fig. 2 consisting of a ground state and well separated one-, two-, three-exciton manifolds, etc., is very general and can be used to describe aggregates of coupled two or three level systems as well as coupled anharmonic vibrations. We consider resonant experiments and only allow transitions between adjacent manifolds which are in resonance with the driving electric field. Therefore, only the single and the two-exciton manifolds contribute to the third order nonlinear response function. By invoking the rotating wave approximation (RWA),[1]

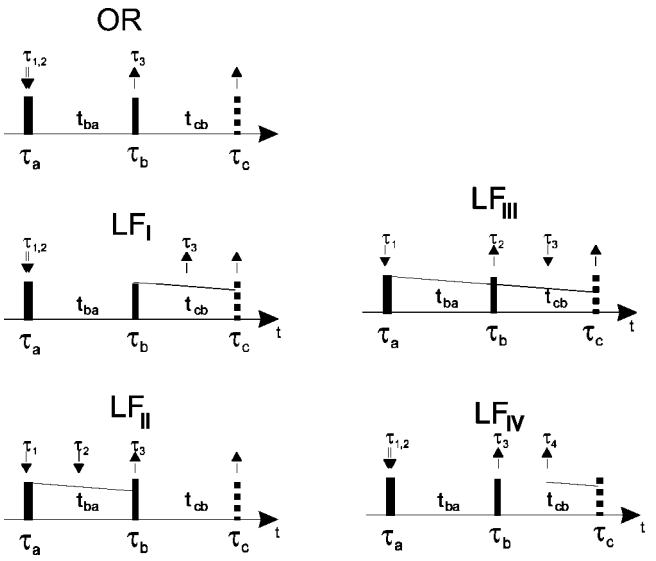

FIG. 1. Schematic representation of the individual terms contributing to the polarization [Eq. (27)]. The vertical bars indicate the pulse sequence, the down (up) arrows correspond to the interaction with the system on the ket- (bra-) side. The decreasing line indicates a FID decay which was initiated by the pulse, where the line starts. See text for details.

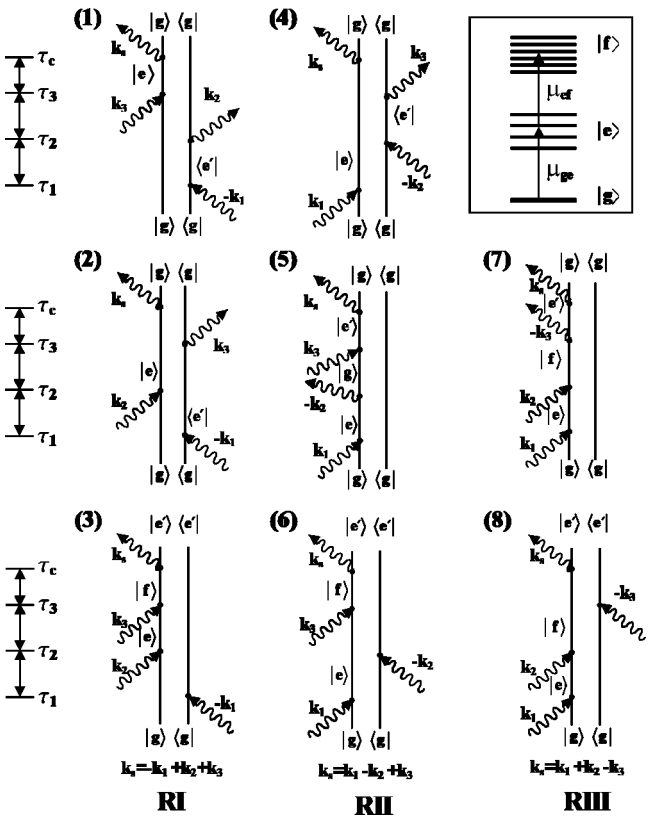

FIG. 2. Double-sided Feynman diagrams representing the Liouville space pathways contributing to the third order response in the rotating wave approximation. Each column shows the diagrams contributing to a four wave mixing signal in a distinct direction $\mathbf{k}_s$, as indicated. τ_1, τ_2, τ_3 are the time-ordered interaction times with the fields. The inset shows the general level scheme.

we find that there are eight Liouville space pathways contributing to the response function. The corresponding Feynman diagrams are shown in Fig. 2.

Four wave mixing signals are generated in several well defined directions, given by the different combinations of the electric field wave vectors.[5] We shall label the pulses in the order they interact with the molecule producing the signal as $\mathbf{k}_1$, $\mathbf{k}_2$, and $\mathbf{k}_3$. If local-field effects are ignored, the external fields directly act on the molecule and the time ordering of the interactions is controlled by the sequence of short non-overlapping pulses. Thus the signal with a wave vector $\mathbf{k}_{RPE}=2\mathbf{k}_a-\mathbf{k}_b$ results exclusively from the pathways producing the polarization in the direction $\mathbf{k}_1+\mathbf{k}_2-\mathbf{k}_3$, i.e., pathways 7 and 8 in Fig. 2. (Note that we assume impulsive pulses and $\tau_a<\tau_b$.)

Our numerical simulations used the sum-over-states expression for the response function given in the following. However, for systems with many chromophores it may be advantageous to calculate the response functions using the nonlinear exciton equations[10,11,28,37–40] which have a more favorable scaling with system size.

We consider an aggregate with the general level scheme shown in the inset of Fig. 2. $|g\rangle$ denotes the ground state, $|e\rangle$, $|e'\rangle\ldots$ the one-exciton states, and $|f\rangle$, $|f'\rangle\ldots$ the two-exciton states. $\varepsilon_{\nu\nu'}$ denotes the energy difference between two states ν and ν'. The transition dipoles between adjacent manifolds are given by μ_{eg} and μ_{fe}. $\Gamma_{\nu'\nu}$ are phenomenological dephasing rates associated with each $\nu'\leftarrow\nu$ transition. For this model the RPE part of the response function responsible for the signal in the $\mathbf{k}_s=\mathbf{k}_1+\mathbf{k}_2-\mathbf{k}_3$ direction contains contributions of diagrams (7) and (8) in Fig. 2[1]

$$
\begin{aligned}
&R^{(3)}_{III}(\tau_c,\tau_3,\tau_2,\tau_1)\\
&\quad=i^3(R_7(\tau_c,\tau_3,\tau_2,\tau_1)+R_8(\tau_c,\tau_3,\tau_2,\tau_1))\\
&\quad=i^3\Theta\rho_0\sum_{e,e',f}\mu_{eg}\mu_{fe}\mu_{fe'}(\mu_{ge'}\\
&\qquad\times\exp[(-i\varepsilon_{e'g}-\Gamma_{e'g})(\tau_c-\tau_3)]-\mu_{e'g}\\
&\qquad\times\exp[(-i\varepsilon_{fe'}-\Gamma_{fe'})(\tau_c-\tau_3)])\\
&\qquad\times\exp[(-i\varepsilon_{fg}-\Gamma_{fg})(\tau_3-\tau_2)]\\
&\qquad\times\exp[(-i\varepsilon_{eg}-\Gamma_{eg})(\tau_2-\tau_1)].
\end{aligned}
\tag{18}
$$

$\Theta\equiv\theta(\tau_c-\tau_3)\theta(\tau_3-\tau_2)\theta(\tau_2-\tau_1)$ stands for the product of Heavyside functions, that ensure proper time ordering within the response function. Note that in Eq. (18) we have explicitly included all three interaction times, even though in this section we assume $\tau_1=\tau_2$, because when local fields are included, this is no longer the case. In the sum the indices e,e' run over all one-exciton states and f runs over all two-exciton states.

The reverse photon-echo signal generated in the direction $\mathbf{k}_{RPE}=2\mathbf{k}_a-\mathbf{k}_b$ is proportional to the nonlinear polarization, which can be calculated from Eqs. (1) and (18), assuming impulsive fields [Eq. (17)],

$$P^{(3)}_{k_{RPE}}(t,\tau_b,\tau_a)=E_a^2E_b^*R^{(3)}_{III}(\tau_c,\tau_b,\tau_a,\tau_a)$$

$$=i^3E_a^2E_b^*\rho_0\sum_{e,e',f}\mu_{eg}\mu_{fe}\mu_{fe'}\mu_{e'g}$$
$$\times(\exp[(-i\varepsilon_{e'g}-\Gamma_{e'g})t_{cb}]$$
$$-\exp[(-i\varepsilon_{fe'}-\Gamma_{fe'})t_{cb}])$$
$$\times\exp[(-i\varepsilon_{fg}-\Gamma_{fg})t_{ba}]. \quad (19)$$

Here $P^{(3)}_{k_{RPE}}$ is the time-resolved polarization component in the $\mathbf{k}_{RPE}$ direction of the general third order polarization ($P^{(3)}(\mathbf{r},t)=\Sigma_i e^{i\mathbf{k}_i\mathbf{r}}P^{(3)}_{ki}(t)$). From Eq. (19) we note that during t_{ba} we have a coherence between a two-exciton state and the ground state, whose phase-oscillation is given by the energy difference of the two-exciton state and the ground state, with dephasing rate Γ_{fg}. The variation of the polarization with t_{ba} will contain the signatures of a superposition of all two-exciton states, which is also retrieved by a Fourier transform (see the following). During t_{cb}, we have two contributions with a similar frequency and a different sign; in the case of an harmonic oscillator with equally spaced energies, these will interfere destructively causing the signal to vanish. This is expected since the harmonic oscillator is linear and has no nonlinear response.[1] Another important point is that all RPE pathways must involve a two-exciton resonance. This is the reason for our earlier statement that no signal is expected for this pulse-configuration for uncoupled two-level systems; within the RWA, a two-level system cannot have two consecutive interactions on the same (bra-, or ket-)side.[7]

Experiments performed on semiconductor quantum wells[21,22] and in the gas phase[23,25] have found a RPE signal. That obviously cannot be explained by the simple picture of electric fields interacting directly with these two band or two level systems. However it is possible to adequately describe these signals using local field effects,[1,7,10,29] as will be shown next.

IV. LOCAL-FIELD EFFECTS IN THE REVERSE PHOTON ECHO

To simplify the discussion of local-field effects, we expand the local field [Eq. (4)] to first order in ρ_0 and the response is then calculated to second order in ρ_0. To first order in ρ_0, Eq. (5) gives in the time domain

$$s(t)=\delta(t)+\frac{4\pi}{3}\rho_0\alpha(t). \quad (20)$$

Using the pulse configuration Eq. (16) and Eq. (4), we obtain for the local field E_l^a associated with the external pulse E^a:

$$E_l^a(\mathbf{r},t)=E^a(\mathbf{r},t)+\frac{4\pi}{3}\rho_0\int\alpha(t-\tau)E^a(\mathbf{r},\tau)d\tau+\text{c.c.}$$

$$=e^{i\mathbf{k_a}\mathbf{r}}\Bigg(E^a(t)+i\theta(t-\tau_a)\frac{4\pi}{3}\rho_0E_a\sum_{e''}\mu^2_{e''g}$$
$$\times\exp[(-i\varepsilon_{e''g}-\Gamma_{eg})(t-\tau_a)]\Bigg)+\text{c.c.} \quad (21)$$

The local field induced by an external short pulse is the sum of the original pulse E^a and the free-induction decay (FID) F^a induced by this pulse.

$$E_l^a(\mathbf{r},t)\equiv E^a(\mathbf{r},t)+F^a(\mathbf{r},t)+\text{c.c.}, \quad (22)$$

where E^a is given by Eq. (17)

$$F^a(\mathbf{r},t)\equiv e^{i\mathbf{k}_a\mathbf{r}}F^a(t)\equiv\frac{4\pi}{3}\rho_0\int\alpha(t-\tau)E^a(\mathbf{r},\tau)d\tau$$
$$=i\theta(t-\tau_a)e^{i\mathbf{k}_a\mathbf{r}}\frac{4\pi}{3}\rho_0E_a\sum_{e''}\mu^2_{e''g}$$
$$\times\exp[(-i\varepsilon_{e''g}-\Gamma_{e''g})(t-\tau_a)]. \quad (23)$$

Here the sum runs over all single exciton states. Note that the free induction decay described by $\alpha(t)$ is initiated *on a different* molecule. This is underlined throughout this article by using a double-prime as a superscript whenever the second system is involved. Static inhomogeneous broadening can be included by replacing this sum with an integration over the inhomogeneous distribution. Note that while E^a is a Delta function $\delta(t-\tau_a)$, F^a has a step function $\theta(t-\tau_a)$ ensuring causality. While E^a represents a short pulse peaking at time $t=\tau_a$, F^a is a superposition of exponential decays starting at $t=\tau_a$ and decaying with the dephasing rates $\Gamma_{e''g}$. This means that for pulse delays shorter than $1/\Gamma_{e''g}$ the time ordering of interactions of the system with the electric field can be reversed compared to the external pulse sequence. The same principle holds in the frequency domain where E^a has a broad spectrum centered at ω_a, while F^a has a Lorentzian line shape, corresponding to the $g\leftarrow e''$ transition.

The total local field E_l is the sum of the contributions of both pulses:

$$E_l(\mathbf{r},t)=E_l^a(\mathbf{r},t)+E_l^b(\mathbf{r},t). \quad (24)$$

E_l enters Eq. (15) in the form of the product $E_l(\tau_1)E_l(\tau_2)E_l(\tau_3)$. Since we are only interested in third-order signals that contain two contributions from the first pulse and one contribution from the second, we only retain products of $E_l^aE_l^aE_l^b$. We further need to sum over all permutations of the time variables τ_1,τ_2,τ_3 since, unlike the Maxwell fields, the local fields are no longer impulsive and time ordering cannot be enforced.

$$E_l(\tau_1)E_l(\tau_2)E_l(\tau_3)=\sum_{\text{perm}}E_l^a(\tau_1)E_l^a(\tau_2)E_l^b(\tau_3). \quad (25)$$

The $\mathbf{k}_{RPE}$ signal must result from terms containing $E_a^2E_b^*$. Furthermore, to second order in ρ_0 we can neglect all terms that contain more than one free-induction contribution (F). This leaves us with

$$E_l(\tau_1)E_l(\tau_2)E_l(\tau_3)$$
$$\approx \sum_{\text{perm}} E^a(\tau_1)E^a(\tau_2)E^{*b}(\tau_3)+E^a(\tau_1)E^a(\tau_2)F^{*b}(\tau_3)$$
$$+2E^a(\tau_1)F^a(\tau_2)E^{*b}(\tau_3)=2E^a(\tau_1)E^a(\tau_2)E^{*b}(\tau_3)$$
$$+2E^a(\tau_1)E^a(\tau_2)F^{*b}(\tau_3)+2E^a(\tau_1)F^a(\tau_2)E^{*b}(\tau_3)$$
$$+2E^a(\tau_1)E^{*b}(\tau_2)F^a(\tau_3), \tag{26}$$

where the second step shows explicitly the permutation of interaction times, taking into account that the impulsive contributions must be time ordered and causality, i.e., the induced FID part can only interact after being generated. In the last term on the r.h.s. of Eq. (26) the interaction time with the field originating from pulses a and b is reversed compared to the pulse sequence. After interacting once with the field, E^a the system subsequently interacts with E^{*b} and finally with F^a, originating from pulse a. Even though the signal is generated in the direction of $\mathbf{k}_{RPE}=2\mathbf{k}_a-\mathbf{k}_b$, in terms of microscopic interactions it is a signal with $\mathbf{k}_s=\mathbf{k}_1-\mathbf{k}_2+\mathbf{k}_3$, resulting from the Liouville space pathways (4)–(6) of Fig. 2 which correspond to a transient grating. Consequently the terms of the response function that need to be taken into account under the RWA are $R_{II}=R_4+R_5+R_6$, rather than pathways R_7 and R_8. The contributions to the nonlinear polarization are schematically shown in Fig. 1.

To second order in ρ_0 we only keep terms with, at most, one FID part. This implies that the time ordering of only one interaction can be delayed and the first interaction still must be from the ket-side. The photon-echo terms (1)–(3) of Fig. 2 do not contribute in this approximation. Using Eq. (15), Eq. (26), and Eq. (20) and retaining terms up to second order in ρ_0, we find that the nonlinear polarization generated at $\mathbf{k}_{RPE}$ has two terms denoted ordinary and local-field induced

$$P^{(3)}_{RPE}(\tau_c,\tau_b,\tau_a)=P^{(3)}_{OR}(\tau_c,\tau_b,\tau_a)+P^{(3)}_{LF}(\tau_c,\tau_b,\tau_a), \tag{27}$$

where

$$P^{(3)}_{OR}(\tau_c,\tau_b,\tau_a)=E_a^2E_b^*R^{(3)}_{III}(\tau_c,\tau_b,\tau_a,\tau_a), \tag{28}$$

$$P^{(3)}_{LF}(\tau_c,\tau_b,\tau_a)\equiv P^{(3)}_{LF_I}(\tau_c,\tau_b,\tau_a)+P^{(3)}_{LF_{II}}(\tau_c,\tau_b,\tau_a)+P^{(3)}_{LF_{III}}(\tau_c,\tau_b,\tau_a)+P^{(3)}_{LF_{IV}}(\tau_c,\tau_b,\tau_a)$$
$$=E_a^2\int_{\tau_b}^{\tau_c}d\tau_3R^{(3)}_{III}(\tau_c,\tau_3,\tau_a,\tau_a)F^{*b}(\tau_3)+2E_aE_b^*\int_{\tau_a}^{\tau_b}d\tau_2R^{(3)}_{III}(\tau_c,\tau_b,\tau_2,\tau_a)F^a(\tau_2)$$
$$+2E_aE_b^*\int_{\tau_b}^{\tau_c}d\tau_3R^{(3)}_{II}(\tau_c,\tau_3,\tau_b,\tau_a)F^a(\tau_3)+E_a^2E_b^*\frac{4\pi}{3}\rho_0\int_{\tau_b}^{\tau_c}d\tau_4\alpha(\tau_c-\tau_4)R^{(3)}_{III}(\tau_4,\tau_b,\tau_a,\tau_a). \tag{29}$$

This is the final expression for the nonlinear polarization generated in the direction of the two-pulse RPE signal calculated using the local-field approximation to first order in the local field and to second order in ρ_0. The five terms represent distinct physical processes, and are schematically depicted in Fig. 1, where the pulse sequence is indicated by the vertical bars and the interactions with the system on the bra- (ket-) side by arrows pointing down (up)wards. The system interacts either directly with the pulse, or with the FID generated by a pulse on *a different* chromophore. This FID is indicated by the decaying line in Fig. 1. The first term [Eq. (28)] corresponds to the ordinary RPE. The last term corresponds to an ordinary RPE signal, that interacts with another molecule and initiates a FID which is detected. Note that in LF_{III} the sequence of interactions is reversed.

Using Eq. (18) for $R^{(3)}_{III}$ and an analogous expression for $R^{(3)}_{II}$ [Eq. (A2)], the time integrations are performed in Appendix A. Numerical results are presented below. The experimental signal can be directly calculated from the polarization [Eq. (27)] for a variety of detection schemes.[1] Mixing the signal with an additional heterodyne pulse at τ_c allows the measurement of the time-resolved polarization, including its phase.[41–43] The heterodyne signal, which depends parametrically on the delay times t_{ba} and t_{cb}, is given by[12]

$$S(t_{cb},t_{ba})=\int_{-\infty}^{\infty}d\tau E_h(\tau)P^{(3)}(\mathbf{r},\tau,\tau_b,\tau_a), \tag{30}$$

where $E_h(\tau)$ is the heterodyne field.

For the following discussion, suffice it to note that both the amplitude and phase of the polarization [Eq. (15)] can be measured experimentally. It may be helpful for the analysis to display the results in the frequency domain by performing a double Fourier transform[5,44,45] The resulting 2D-FT signal[12] is then given by

$$S(\Omega_2,\Omega_1)=\int_0^{\infty}dt_{cb}\int_0^{\infty}dt_{ba}S(t_{cb},t_{ba})$$
$$\times\exp[i\Omega_2t_{cb}+i\Omega_1t_{ba}]. \tag{31}$$

We shall use this representation to display our results. Note that Ω_1 is the frequency conjugate to t_{ba} and Ω_2 is conjugate to t_{cb}. Ω_1 thus reflects the dynamics taking place between the two pulses, while Ω_2 shows the evolution after the second pulse.

V. RPE SIGNALS FOR TWO AND THREE LEVEL MODEL SYSTEMS

In this section we present the RPE signal [Eq. (31)] for various model systems with the goal of clearly highlighting the many-body resonances. Although local fields can induce new peaks, they do not carry new microscopic information, unlike the peaks caused by microscopic couplings. The important differences between the two will be discussed for a few examples, using typical parameters for IR spectroscopy of anharmonic vibrations.

In all the numerical calculations we assumed equal one-exciton transition dipoles μ_{eg} and dephasing constants Γ_{eg}. From Eq. (A6) and Eqs. (A7)–(A10) [or similar Eq. (A11) and Eqs. (A12)–(A15)] we can see that in this case the ratio of the first and second order terms in ρ_0 (the ordinary RPE and the local field-induced signal) is determined by a factor of $(4\pi)/3\,\rho_0|\mu_{eg}|^2$, which has the same dimensions (of energy) as Γ_{eg}. This factor was assumed to be $0.1\Gamma_{eg}$ in all calculations for illustration purposes. Based on crude estimates, we expect this low order truncation in ρ_0 to hold even for neat liquids.

In the case of very high chromophore density and strong oscillator strengths, an expansion to higher order would be straightforward. An expansion of the local field in ρ_0 could be totally avoided, by calculating $s(t)$ via a numerical Fourier transform directly from Eq. (5). However, the perturbative expansion is extremely valuable, since it allows us to distinguish the different effects and clarify their origin, as shown in the following.

A. Uncoupled two level systems

As discussed in the previous section, for a collection of uncoupled two level systems the response-function contributions for $\mathbf{k}_{RPE}$ vanish ($R^{(3)}_{III}=0$) and no RPE signal is generated in the direction $2\mathbf{k}_a-\mathbf{k}_b$. However, Eq. (27) also contains a purely local-field contribution, which depends on $R^{(3)}_{III}$ and $R^{(3)}_{II}$ [Eq. (29)]. The expression for $R^{(3)}_{II}$ becomes particularly simple in the present model, since it is the sum of the individual response functions. Only the third term on the r.h.s. of Eq. (29) is nonzero. Neglecting evolution in the excited- or ground-state population periods, we get from Eq. (A9)

$$P^{(3)2LS}_{ks}(t_{cb},t_{ba})=i^3\frac{4\pi}{3}\rho_0^2\sum_{e'',e}|\mu_{e''g}|^2|\mu_{eg}|^4E_a^2E_b^*\exp[(-i(\varepsilon_{e''g}+\varepsilon_{eg})-(\Gamma_{e''g}+\Gamma_{eg}))t_{ba}]$$
$$\times\frac{\exp[(-i\varepsilon_{e''g}-\Gamma_{e''g})t_{cb}]-\exp[(-i\varepsilon_{eg}-\Gamma_{eg})t_{cb}]}{\varepsilon_{eg}-\varepsilon_{e''g}+i(\Gamma_{e''g}-\Gamma_{eg})}, \tag{32}$$

where we wrote the signal which is *exclusively induced by the local field* as a function of the time delays (t_{cb}, t_{ba}) and the sum runs over all different pairs of molecules. From Eq. (32) we clearly deduce the expected effects and their difference from two-exciton resonances resulting from direct coupling. The most interesting temporal evolution occurs during t_{ba} where the signal shows oscillations at sums of single-exciton energies. During this period, two molecules are in a coherence and the many-body density matrix oscillates at the sum of their frequencies.[29] The observed frequencies are therefore simple sums of one-exciton resonance frequencies, no multiple quantum coherence between separated molecules is involved, and the new resonances carry no additional microscopic information. This is in contrast to multiple quantum resonances resulting from intermolecular coupling (vide infra), where oscillations at frequencies of ε_{fg} are observed during the period t_{ba}. Also the relaxation during this time interval is given by the sum of one-exciton damping rates $(\Gamma_{eg}+\Gamma_{e''g})$. This doubling of the dephasing rate was observed experimentally in semiconductor quantum wells.[21,22] During the time period t_{cb}, the system oscillates at a superposition of single-exciton frequencies.

In the special case of a sample of identical uncoupled two level systems, Eq. (32) reduces to

$$P^{(3)TLS}_{ks}(t_{cb},t_{ba})=i^4\frac{4\pi}{3}\rho_0^2|\mu_{eg}|^6E_a^2E_b^*t_{cb}$$
$$\times\exp[(-i\varepsilon_{eg}-\Gamma_{eg})t_{cb}]$$
$$\times\exp[(-i2\varepsilon_{eg}-2\Gamma_{eg})t_{ba}], \tag{33}$$

where we used the limit

$$\lim_{\bar{\epsilon}_2\to\bar{\epsilon}_1}\left(\frac{\exp[-i\bar{\epsilon}_1t]-\exp[-i\bar{\epsilon}_2t]}{\bar{\epsilon}_2-\bar{\epsilon}_1}\right)=it\exp[-i\bar{\epsilon}_1t]. \tag{34}$$

Even though the denominator of Eq. (32) vanishes, the limit in Eq. (34) is well-defined and leads to a secular contribution initially increasing linearly with t_{cb}. $P^{(3)}$ does not diverge, because of the exponential damping term $e^{-\Gamma_{eg}t_{cb}}$. When inhomogeneous broadening is included, we need to integrate Eq. (32) over distributions of energies which can further cure this divergence. The simple linear rise with time results from the neglect of population decay ($\Gamma_{ee}=\Gamma_{gg}=0$) and static broadening, so that the FID is *exactly* on resonance with the $e\leftarrow g$ transition. This problem does not occur if a more realistic relaxation model is included. (See page 167 of Ref. 1.)

The physical meaning of the initial rise of the signal during t_{cb} can be understood from Fig. 1. For a two level

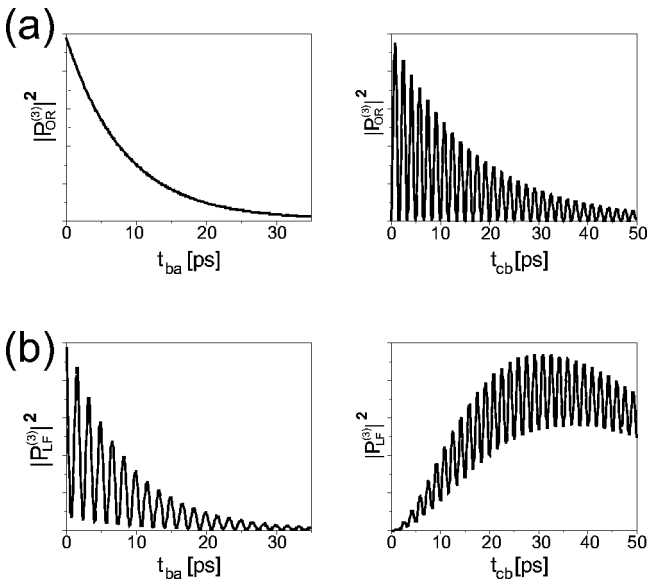

FIG. 3. The squares of the amplitudes of (a) the ordinary RPE contributions and (b) the local field contributions to the time-resolved RPE signal of a three level system as a function of t_{ba} (with $t_{cb}=11$ ps) and t_{cb} (with $t_{ba}=0$) in the first and second column, respectively.

system, the entire signal results from the LF_{III} term, where the time ordering of interactions is reversed with respect to the pulse-delay times and the last interaction is with the FID initiated by the first pulse and takes place after the second pulse. The larger the t_{cb}, the more time there is for this interaction to occur. Note also that after the interaction with the second pulse at τ_b, the system is in a population state. In the absence of population relaxation, the only contributions to the decay of the signal is the decay of the FID that interacts with the system, and after the interaction, the decay of the generated signal. Since for our simple two level system these two contributions have the same relaxation rate (because the FID, as well as the final signal results from the same transition), we get the simple $t_{cb}e^{-\Gamma t_{cb}}$ behavior in Eq. (33). This initial rise as a function of t_{cb} is only seen in the local-field contributions but not in the ordinary RPE signal.

From Eq. (33), we expect the polarization as a function of t_{ba} to oscillate with twice the optical frequency and decay with $2\Gamma_{eg}$. Homodyne detected experiments measure the time integrated signal $S^H_A(t_{ba})=\int_0^\infty dt_{cb}|P_A(t_{cb},t_{ba})|^2$ and in this case we expect the signal to be proportional to $e^{-4\Gamma_{eg}t_{ba}}$. This effect of fast dephasing with twice the rate of a photon echo experiment was observed in semiconductor quantum wells.[21] Using heterodyned detection it should be possible to directly observe the high harmonic frequency corresponding to twice the optical transition energy.

The time-resolved ordinary RPE signal and the local-field contributions for a three level system are compared in Fig. 3, where we used a three level system because for a two level system no ordinary RPE contribution exists. The two columns show the squared amplitude of the polarization as a function of t_{ba} and t_{cb} (with the other time variable held fixed), respectively. While the ordinary RPE signal only shows exponential decay, the local field contribution (which for a three level system consists of a superposition of several contributions) initially increases as a function of t_{cb}. The parameters used are the same as for the three level system described following. The oscillation results from beating of the $f\leftarrow e$ and $e\leftarrow g$ transitions and has a period of 1.7 ps, corresponding to the anharmonicity ($\Delta=\varepsilon_{eg}-\varepsilon_{fe}=20\ \mathrm{cm}^{-1}$).

As discussed previously, for two level systems the $\mathbf{k}_{RPE}$ signal can be generated either by local-field effects or by intermolecular coupling.[29] Let us compare the local-field effects to the ordinary RPE signal for a simple model of two strongly coupled two level systems. The level scheme schematically depicted in the inset of Fig. 4(b) consists of a ground state $|g\rangle$, two single excited states $|e+\rangle$, $|e-\rangle$ with an energy spacing depending on the coupling J, and one doubly excited state $|f\rangle$. These states are obtained by diagonalizing the 4×4 Hamiltonian of this system.

The polarization responsible for the ordinary RPE $2\mathbf{k}_a-\mathbf{k}_b$ signal for two coupled two level systems (Fig. 4) is

$$P^{(3)cTLS}_{OR}(t_{cb},t_{ba})$$
$$=i^3\frac{4\pi}{3}\rho_0^2E_a^2E_b^*(\mu_{e-,g}\mu_{f,e-}+\mu_{e+,g}\mu_{f,e+})$$
$$\times\sum_{e=e-,e+}\mu_{eg}\mu_{fe}e^{(-i\varepsilon_{fg}-\Gamma_{fg})t_{ba}}$$
$$\times[e^{(-i\varepsilon_{eg}-\Gamma_{eg})t_{cb}}-e^{(-i\varepsilon_{fe}-\Gamma_{fe})t_{cb}}]. \quad (35)$$

This is markedly different from the local-field signal [Eq. (32)], where all combinations of one exciton frequencies (including $2\varepsilon_{eg}$) contribute to the signal in t_{ba}. This is shown in Fig. 4(a), which displays the 2D signal for two independent two level systems. Figure 4 compares the local field induced RPE signal of two independent two level systems with the ordinary RPE signal caused by the coupling between two interacting two level systems. The parameters used in the simulations were: $\varepsilon_{e1,g}=2014\,\mathrm{cm}^{-1}$, $\varepsilon_{e2,g}=2085\ \mathrm{cm}^{-1}$, the transition dipole moments μ as well as the damping $\Gamma=1\mathrm{cm}^{-1}$ of the independent two level systems were assumed to be equal. For the coupled system we assumed a coupling constant $J=-10\ \mathrm{cm}^{-1}$. The dephasing rates for the coupled system were set to $\Gamma_{eg}=\Gamma_{fe}=1\ \mathrm{cm}^{-1}$ (for $e=e-,e+$), $\Gamma_{fg}=2\Gamma_{eg}$.

As can be seen in Fig. 4(b) the ordinary RPE signal [Eq. (35)] only shows peaks when Ω_1 is resonant with the two-exciton state. It thus provides new microscopic information about the two-exciton manifold. The structure of Eq. (35) coincides with the case of two three-level systems with identical ε_{fg} and an amplitude ratio $A_1/A_2=(\mu_{e1g}\mu_{fe1})/(\mu_{e2g}\mu_{fe2})$ (as discussed in the next section). In principle it should also be possible to distinguish between resonances induced by coupling between different sites and intramolecular resonances of a three-level system. In a four wave mixing experiment with three different pulses they should have different phases as a function of the time delay between the first two interactions which is set to zero in the present calculations.

The phase profiles of the local field-induced and ordinary RPE resonances displayed in the second column of Fig.

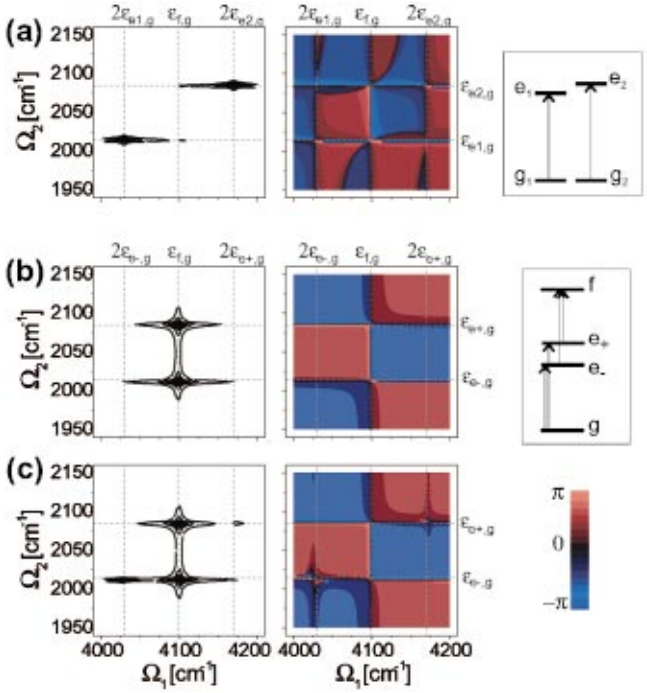

FIG. 4. (Color) (a) The total local field-induced RPE signal of a system composed of two independent two level systems (b) the ordinary RPE and (c) the total RPE signal (including local-field effects) for two coupled two level systems. The first two columns show the amplitude and phase, respectively of the 2D-FT signal. The dotted lines indicate the relevant transition energies (see text). The insets in the last column show the corresponding level schemes. The parameters for the two level systems used in the simulations were: $\varepsilon 1_{eg}=2014\ \mathrm{cm}^{-1}$, $\varepsilon 2_{eg}=2085\ \mathrm{cm}^{-1}$, the transition dipole moments of the independent two level systems were assumed to be equal and the damping $\Gamma=1\mathrm{cm}^{-1}$. For the coupled system we assumed coupling constant $J=-10\ \mathrm{cm}^{-1}$ between the two systems.

4 show pronounced differences. Equation (35) represents the pure RPE without local-field contributions. In general we should see a superposition of resonances caused by coupling and by local field, and this case is shown in Fig. 4(c). New peaks can be found at $\Omega_1=2\varepsilon_{e1,g}$ and $\Omega_1=2\varepsilon_{e2,g}$. The

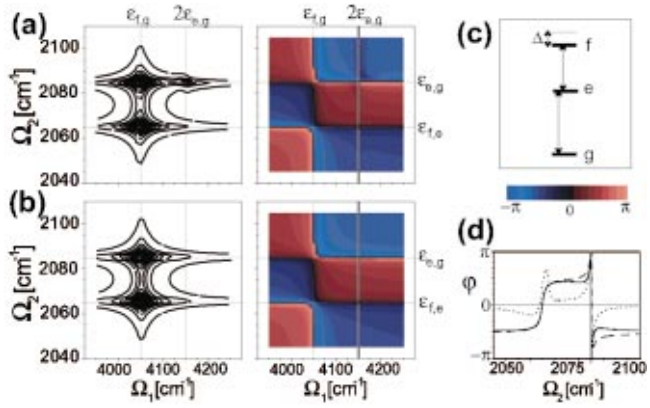

FIG. 5. (Color) (a) total RPE signal and (b) the ordinary RPE contributions for a three level model with the parameters as indicated in the text. The first column shows the amplitude and the second column the phase of the signal. The dotted lines indicate the relevant transition energies at ε_{eg}, ε_{fe} and $2\varepsilon_{eg}$, ε_{fg}. (c) The level scheme and (d) a slice through the 2D-phase plot at $\Omega_1=2\varepsilon_{eg}$ showing the total signal (solid), ordinary RPE signal (dashed) and local-field contributions (dotted).

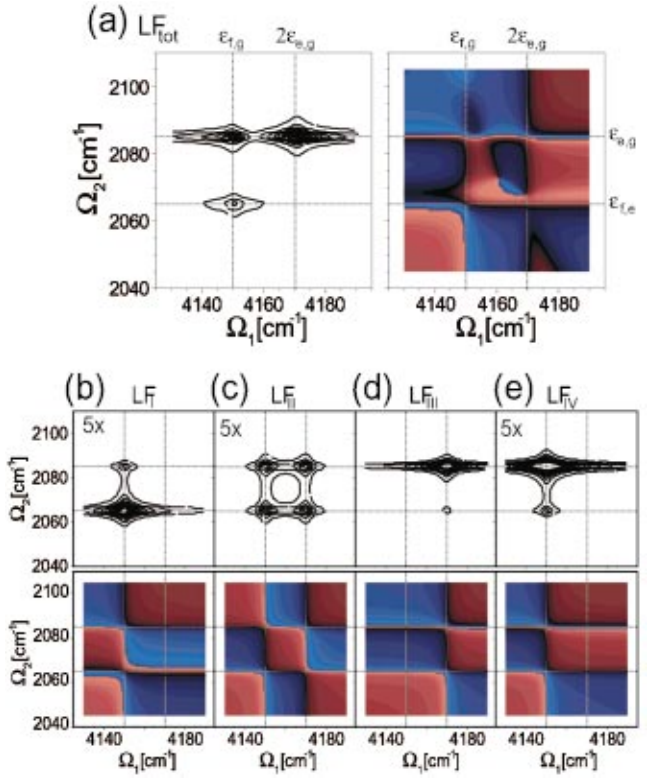

FIG. 6. (Color) Local-field effects for a three level system: (a) amplitude and phase of the total local field contributions. (b)–(e) The individual contributions. The diagrams for LF_I, LF_{II}, and LF_{IV} are multiplied by a factor of 5 with respect to LF_{III}.

local-field contributions will have a different dependence on molecular density and a different profile of the phase.

B. Identical three level systems

A system of identical uncoupled three level chromophores whose level scheme is shown in the inset of Fig. 5, is the simplest model where all terms of Eq. (27) contribute. We assume a ground state $|g\rangle$, a first excited state $|e\rangle$ and a second excited state $|f\rangle$ with an anharmonicity $\Delta=\varepsilon_{eg}-\varepsilon_{fe}$. We further neglect population relaxation ($\Gamma_{ee}=0$) but keep all other dephasing rates general. The following parameters were used in the simulations: $\varepsilon_{eg}=2085\ \mathrm{cm}^{-1}$, $\varepsilon_{fg}=4150\ \mathrm{cm}^{-1}$, $\Delta=20\ \mathrm{cm}^{-1}$, $\mu_{fe}=1.3\mu_{eg}$, $\Gamma=1\ \mathrm{cm}^{-1}$.

For this model the polarization [Eq. (27)] can be calculated analytically and we next discuss the various effects in more detail.

1. Ordinary RPE signal of a three level system

The time domain RPE signal resulting from the impulsive fields alone is determined by the polarization [Eq. (A6)]

$$P_{OR}^{(3)3LS}(t_{cb},t_{ba})=i^3\rho_0E_a^2E_b^*|\mu_{eg}|^2|\mu_{fe}|^2e^{(-i\varepsilon_{fg}-\Gamma_{fg})t_{ba}}\times[e^{(-i\varepsilon_{eg}-\Gamma_{eg})t_{cb}}-e^{(-i\varepsilon_{fe}-\Gamma_{fe})t_{cb}}]. \quad (36)$$

The two terms oscillating at frequencies $(\varepsilon_{fg},\varepsilon_{eg})$ and $(\varepsilon_{fg},\varepsilon_{fe})$ as a function of (t_{ba},t_{cb}) can be clearly seen. Note that due to the minus sign, the two terms will exactly cancel for a system with vanishing anharmonicty $\Delta=0$ and equal damping $\Gamma_{eg}=\Gamma_{fe}$. The two resonances are recovered in the

2D-FT signal, shown in Fig. 5 which compares the total signal including local-field effects, with the ordinary RPE signal. The Fourier transform can be performed analytically and from Eq. (A11) we get

$$S_{OR}^{3LS}(\Omega_2,\Omega_1)=i^3\rho_0 E_a^2 E_b^* \mu_{eg}^2\mu_{fe}^2 \times\left[\frac{1}{(\Omega_2-\varepsilon_{eg}+i\Gamma_{eg})(\Omega_1-\varepsilon_{fg}+i\Gamma_{fg})} - \frac{1}{(\Omega_2-\varepsilon_{fe}+i\Gamma_{fe})(\Omega_1-\varepsilon_{fg}+i\Gamma_{fg})}\right]. \quad (37)$$

While the ordinary RPE signal only shows resonances $\Omega_1=\varepsilon_{fg}$, inclusion of local fields leads to new peaks at $\Omega_1=2\varepsilon_{eg}$. Also the phase profile is different and the local field influences and modifies the original resonances. This can be clearly seen in Fig. 5(d), where the phase variation along a slice with $\Omega_1=2\varepsilon_{eg}$ is shown for the total RPE signal, the ordinary RPE and the LF contribution.

When examining the variation with different delay times, we note that as a function of t_{ba} the polarization is a damped oscillation with frequency ε_{fg} and a phase determined by the second delay period t_{cb}, whereas as a function of t_{cb}, the signal shows an amplitude modulation with a beat frequency corresponding to the anharmonicity. As a function of t_{ba} we expect a single damped oscillation. The homodyne signal of our simple model should show an exponential decay proportional to $e^{-2\Gamma_{fg}t_{ba}}$ (cf. Fig. 3).

2. Local field effects

The local field induced terms [Eq. (29)] are evaluated in Appendix A [Eqs. (A7)–(A9)] and expressions for the three level system can be easily obtained. These terms correspond to the different LF contributions as schematically sketched in Fig. 1. Figure 6 shows the absolute value and the phase of the total local-field contribution and of each of the individual contributions to the 2D-FT RPE signal. The first term describes the time ordering, where the first pulse interacts twice with the system and the final interaction occurs with the FID generated on another chromophore by the last pulse.

$$P_{LF_I}^{(3)3LS}(t_{cb},t_{ba})=i^3\frac{4\pi}{3}\rho_0^2E_a^2E_b^*|\mu_{eg}|^4|\mu_{fe}|^2 e^{(-i\varepsilon_{fg}-\Gamma_{fg})t_{ba}} \times\left[\frac{e^{(-i\varepsilon_{fe}-(\Gamma_{fg}+\Gamma_{eg}))t_{cb}}-e^{(-i\varepsilon_{eg}-\Gamma_{eg})t_{cb}}}{(\varepsilon_{eg}-\varepsilon_{fe})+i\Gamma_{fg}} + \frac{e^{(-i\varepsilon_{fe}-\Gamma_{fe})t_{cb}}-e^{(-i\varepsilon_{fe}-(\Gamma_{fg}+\Gamma_{eg}))t_{cb}}}{i(\Gamma_{fg}+\Gamma_{eg}-\Gamma_{fe})}\right]. \quad (38)$$

In Fig. 6(b) we see two peaks at $(\varepsilon_{fg},\varepsilon_{eg})$ and $(\varepsilon_{fg},\varepsilon_{fe})$ for LF_I and Eq. (38) shows that they result from the superposition of different contributions. As in the pure RPE case, all resonances occur at $\Omega_1=\varepsilon_{fg}$ and as a function of t_{ba}, Eq. (38) is similar to Eq. (36), as far as frequency and damping are concerned, but has a different phase because of the different variation with t_{cb}. The denominators in the r.h.s. of Eq. (38) add complex amplitudes to the terms, which depend on the damping and the anharmonicity. This term results from the interaction of the FID with the system. Since the FID is caused by a $g\leftarrow e$ transition of another (identical) molecule, it can only be resonant with ε_{eg} and is detuned by Δ from the $f\leftarrow e$ transition. For the last two terms the real part of the denominator vanishes (since for our model, which neglects inhomogeneous broadening, the FID is *exactly* on resonance). However, the dephasing rates do not generally cancel and will give a purely imaginary prefactor. For zero anharmonicity and equal damping the entire term vanishes.

2D-Fourier transform of Eq. (38) gives

$$S_{LF_I}^{3LS}(\Omega_2,\Omega_1) =i^3\frac{4\pi}{3}\rho_0^2E_a^2E_b^*|\mu_{eg}|^4|\mu_{fe}|^2 \times\frac{1}{\Omega_1-\varepsilon_{fg}+i\Gamma_{fg}}\left\{\frac{1}{(\varepsilon_{eg}-\varepsilon_{fe})+i\Gamma_{fg}} \times\left[\frac{1}{\Omega_2-\varepsilon_{fe}+i(\Gamma_{fg}+\Gamma_{eg})}-\frac{1}{\Omega_2-\varepsilon_{eg}+i\Gamma_{eg}}\right] - \frac{1}{i(\Gamma_{fg}+\Gamma_{eg}-\Gamma_{fe})} \times\left[\frac{1}{\Omega_2-\varepsilon_{fe}+i(\Gamma_{fg}+\Gamma_{eg})}-\frac{1}{\Omega_2-\varepsilon_{fe}+i\Gamma_{fe}}\right]\right\}. \quad (39)$$

The next term corresponds to the process where the system interacts once with pulse one, then with the FID of another molecule induced by pulse one and finally with the second pulse at τ_b. As in the above-mentioned case the time ordering is not reversed with respect to the ordinary RPE.

$$P_{LF_{II}}^{(3)3LS}(t_{cb},t_{ba})=2i^3\frac{4\pi}{3}\rho_0^2E_a^2E_b^*|\mu_{eg}|^4|\mu_{fe}|^2 \times\frac{1}{\varepsilon_{fg}-2\varepsilon_{eg}+i(2\Gamma_{eg}-\Gamma_{fg})} \times\{e^{(-i2\varepsilon_{eg}-2\Gamma_{eg})t_{ba}}[e^{(-i\varepsilon_{eg}-\Gamma_{eg})t_{cb}} - e^{(-i\varepsilon_{fe}-\Gamma_{fe})t_{cb}}]-e^{(-i\varepsilon_{fg}-\Gamma_{fg})t_{ba}} \times[e^{(-i\varepsilon_{eg}-\Gamma_{eg})t_{cb}}-e^{(-i\varepsilon_{fe}-\Gamma_{fe})t_{cb}}]\} \quad (40)$$

This term is interesting because it shows four resonances with all combinations of $\Omega_1=\varepsilon_{fg}$ or $2\varepsilon_{eg}$ and $\Omega_2=\varepsilon_{eg}$ or ε_{fe} as can be seen in Fig. 6(c). They all have the same amplitude which depends on detuning. Note that as long as $\Delta\neq 0$, the real part of the denominator does not vanish. This is why this term generally makes only a minor contribution. Again, for vanishing anharmonicity (and equal damping) this term vanishes.

In the frequency domain this signal is

$$S^{3LS}_{LF_{II}}(\Omega_2,\Omega_1)=2i^3\frac{4\pi}{3}\rho_0^2E_a^2E_b^*|\mu_{eg}|^4|\mu_{fe}|^2 \times\frac{1}{\varepsilon_{fg}-2\varepsilon_{eg}+i(2\Gamma_{eg}-\Gamma_{fg})} \times\left\{\frac{1}{\Omega_1-2\varepsilon_{eg}+i2\Gamma_{eg}}\left[\frac{1}{\Omega_2-\varepsilon_{eg}+i\Gamma_{eg}} -\frac{1}{\Omega_2-\varepsilon_{fe}+i\Gamma_{fe}}\right)\right]-\frac{1}{\Omega_1-\varepsilon_{fg}+i\Gamma_{fg}} \times\left[\frac{1}{\Omega_2-\varepsilon_{eg}+i\Gamma_{eg}}-\frac{1}{\Omega_2-\varepsilon_{fe}+i\Gamma_{fe}}\right]. \quad (41)$$

The next term is very special since it is the only one that involves a reversal in the order of interactions. First, the system interacts with the first pulse from the bra-, then with the second pulse from the ket- side and finally with the FID of another molecule, initiated by the first pulse. In this case the system is never prepared in a coherent superposition of $|f\rangle$ and $|g\rangle$ and shows no resonances at $\Omega_1=\varepsilon_{fg}$ in Fig. 6(c). But after the first pulse, two separated uncoupled molecules are excited coherently and interact after the second pulse via the FID.

As shown above, for uncoupled two level systems this term is the only one contributing in the direction $2\mathbf{k}_{RPE}$. For the three level case we get from Eq. (A9)

$$P^{(3)3LS}_{LF_{III}}(t_{cb},t_{ba})=2i^3\frac{4\pi}{3}\rho_0^2E_a^2E_b^*|\mu_{eg}|^4e^{(-i2\varepsilon_{eg}-2\Gamma_{eg})t_{ba}} \times\left[2|\mu_{e'g}|^2it_{cb}e^{(-i\varepsilon_{eg}-\Gamma_{eg})t_{cb}} -|\mu_{fe}|^2\frac{e^{(-i\varepsilon_{eg}-\Gamma_{eg})t_{cb}}-e^{(-i\varepsilon_{fe}-\Gamma_{fe})t_{cb}}}{\varepsilon_{fe}-\varepsilon_{eg}+i(\Gamma_{eg}-\Gamma_{fe})}\right]. \quad (42)$$

We find that all resonances occur at $\Omega_1=2\varepsilon_{eg}$. The main contribution arises from the first term on the r.h.s. whereby the FID is exactly on resonance with the induced transitions. This term peaks at $(\Omega_1,\Omega_2)=(2\varepsilon_{eg},\varepsilon_{eg})$; no double-exciton state is involved. The other two terms, peaking also at $(2\varepsilon_{eg},\varepsilon_{eg})$, as well as at $(\varepsilon_{fg},\varepsilon_{eg})$, contain a complex prefactor with the detuning in the denominator, making them small compared to the first term. Note that for special values of damping (i.e., when $\Gamma_{eg}-\Gamma_{fe}=\Gamma_{fg}-2\Gamma_{eg}$) they cancel exactly with the first term on the r.h.s. of Eq. (40). Equation (42) only vanishes for the harmonic case, i.e., when the transition energy and the dephasing rates are equal for the $e\leftarrow g$ and $f\leftarrow e$ transitions *and* the dipole moments correspond to the harmonic case ($\mu_{fe}=\sqrt{2}\mu_{eg}$).[46] In the frequency domain this signal is

TABLE I. Contributions to the four peaks in the signal of a three level system. For each resonance peak, all contributions are listed, showing which term contributes the prefactor and the dephasing characteristics of each contribution. $\lambda\equiv i^3E_a^2E_b^*|\mu_{eg}|^2|\mu_{fe}|^2$, $\lambda'\equiv i^3\,4\pi/3\,E_a^2E_b^*|\mu_{eg}|^4|\mu_{fe}|^2$, and $\lambda''\equiv i^3\,4\pi/3\,E_a^2E_b^*|\mu_{eg}|^6$.

Resonance	Contribution	Prefactor	Damping
$(\varepsilon_{fg},\varepsilon_{eg})$	OR	$\lambda\rho_0$	$(\Gamma_{fg},\Gamma_{eg})$
$(\varepsilon_{fg},\varepsilon_{eg})$	LF_I	$-\lambda'\rho_0^2/(\Delta+i\Gamma_{fg})$	$(\Gamma_{fg},\Gamma_{eg})$
$(\varepsilon_{fg},\varepsilon_{eg})$	LF_{II}	$-2\lambda'\rho_0^2/(-\Delta+i(2\Gamma_{eg}-\Gamma_{fg}))$	$(\Gamma_{fg},\Gamma_{eg})$
$(\varepsilon_{fg},\varepsilon_{eg})$	LF_{IV}	$i\lambda'\rho_0^2t_{cb}$	$(\Gamma_{fg},\Gamma_{eg})$
$(\varepsilon_{fg},\varepsilon_{eg})$	LF_{IV}	$\lambda'\rho_0^2/(\Delta+i(\Gamma_{fe}-\Gamma_{eg}))$	$(\Gamma_{fg},\Gamma_{eg})$
$(\varepsilon_{fg},\varepsilon_{fe})$	OR	$\lambda\rho_0$	$(\Gamma_{fg},\Gamma_{fe})$
$(\varepsilon_{fg},\varepsilon_{fe})$	LF_I	$\lambda'\rho_0^2/(\Delta+i\Gamma_{fg})$	$(\Gamma_{fg},\Gamma_{fg}+\Gamma_{eg})$
$(\varepsilon_{fg},\varepsilon_{fe})$	LF_I	$\lambda'\rho_0^2/(i(\Gamma_{fg}+\Gamma_{eg}-\Gamma_{fe}))$	$(\Gamma_{fg},\Gamma_{fe})$
$(\varepsilon_{fg},\varepsilon_{fe})$	LF_I	$-\lambda'\rho_0^2/(i(\Gamma_{fg}+\Gamma_{eg}-\Gamma_{fe}))$	$(\Gamma_{fg},\Gamma_{fg}+\Gamma_{eg})$
$(\varepsilon_{fg},\varepsilon_{fe})$	LF_{II}	$2\lambda'\rho_0^2/(-\Delta+i(2\Gamma_{eg}-\Gamma_{fg}))$	$(\Gamma_{fg},\Gamma_{eg})$
$(\varepsilon_{fg},\varepsilon_{fe})$	LF_{IV}	$-\lambda'\rho_0^2/(\Delta+i(\Gamma_{fe}-\Gamma_{eg}))$	$(\Gamma_{fg},\Gamma_{eg})$
$(2\varepsilon_{eg},\varepsilon_{eg})$	LF_{II}	$2\lambda'\rho_0^2/(-\Delta+i(2\Gamma_{eg}-\Gamma_{fg}))$	$(2\Gamma_{eg},\Gamma_{eg})$
$(2\varepsilon_{eg},\varepsilon_{eg})$	LF_{III}	$2i\lambda''\rho_0^2t_{cb}$	$(2\Gamma_{eg},\Gamma_{eg})$
$(2\varepsilon_{eg},\varepsilon_{eg})$	LF_{III}	$-2\lambda'\rho_0^2/(-\Delta+i(\Gamma_{eg}-\Gamma_{fe}))$	$(2\Gamma_{eg},\Gamma_{eg})$
$(2\varepsilon_{eg},\varepsilon_{fe})$	LF_{II}	$-2\lambda'\rho_0^2/(-\Delta+i(2\Gamma_{eg}-\Gamma_{fg}))$	$(2\Gamma_{eg},\Gamma_{fe})$
$(2\varepsilon_{eg},\varepsilon_{fe})$	LF_{III}	$2\lambda'\rho_0^2/(-\Delta+i(\Gamma_{eg}-\Gamma_{fe}))$	$(2\Gamma_{eg},\Gamma_{fe})$

$$S^{3LS}_{LF_{III}}(\Omega_2,\Omega_1)=2i^3\frac{4\pi}{3}\rho_0^2E_a^2E_b^*|\mu_{eg}|^4 \times\frac{1}{\Omega_1-2\varepsilon_{eg}+i2\Gamma_{eg}}\left\{\frac{2|\mu_{eg}|^2}{(\Omega_2-\varepsilon_{eg}+i\Gamma_{eg})^2} -\frac{|\mu_{fe}|^2}{\varepsilon_{fe}-\varepsilon_{eg}+i(\Gamma_{eg}-\Gamma_{fe})}\left[\frac{1}{\Omega_2-\varepsilon_{eg}+i\Gamma_{eg}} -\frac{1}{\Omega_2-\varepsilon_{fe}+i\Gamma_{fe}}\right]\right\}. \quad (43)$$

Finally, to take all local field effects into account, we have to consider the contributions of processes whereby after creating the RPE signal by three interactions with the pulses the generated signal interacts with another molecule to generate a FID which is finally detected. For the three level system this term gives

$$P^{(3)3LS}_{LF_{IV}}(t_{cb},t_{ba})=i^3\frac{4\pi}{3}\rho_0^2E_a^2E_b^*|\mu_{eg}|^4|\mu_{fe}|^2e^{(-i\varepsilon_{fg}-\Gamma_{fg})t_{ba}} \times\left\{it_{cb}e^{(-i\varepsilon_{eg}-\Gamma_{eg})t_{cb}} -\frac{1}{\varepsilon_{eg}-\varepsilon_{fe}+i(\Gamma_{fe}-\Gamma_{eg})} \times[e^{(-i\varepsilon_{fe}-\Gamma_{fe})t_{cb}}-e^{(-i\varepsilon_{eg}-\Gamma_{eg})t_{cb}}]\right\}. \quad (44)$$

Not surprisingly, we find only resonances with $\Omega_1=\varepsilon_{fg}$ and the major contribution at $(\varepsilon_{fg},\varepsilon_{eg})$. In the frequency domain we obtain

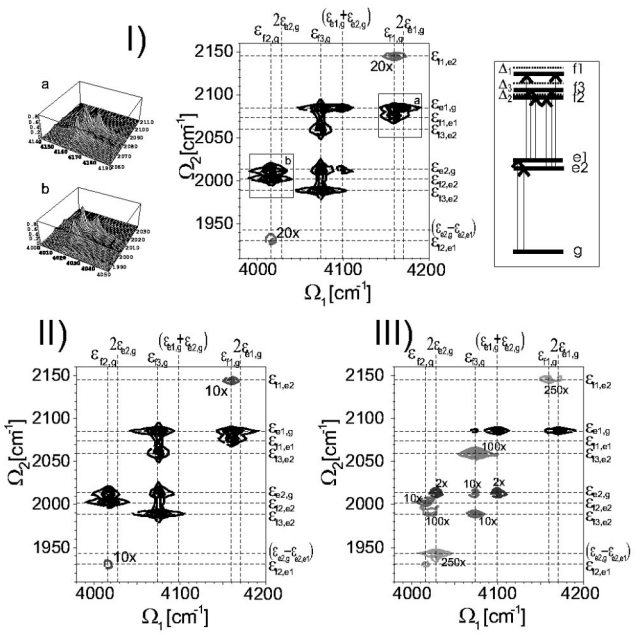

FIG. 7. The amplitude of the 2D-FT signal for two coupled three level systems as shown in the inset. (I) The total signal, which consists of the ordinary RPE (II) and the local-field contributions (III). Smaller peaks are zoomed out by the factors indicated. The two indicated regions of (I) are shown in a 3D plot on the left side.

$$S^{3LS}_{LF_{IV}}(\Omega_2,\Omega_1)=i^3\frac{4\pi}{3}\rho_0^2E_a^2E_b^*|\mu_{eg}|^4|\mu_{fe}|^2\frac{1}{\Omega_1-\varepsilon_{fg}+i\Gamma_{fg}}$$
$$\times\left\{\frac{1}{(\Omega_2-\varepsilon_{eg}+i\Gamma_{eg})^2}\right.$$
$$-\frac{1}{\varepsilon_{eg}-\varepsilon_{fe}+i(\Gamma_{fe}-\Gamma_{eg})}\left[\frac{1}{\Omega_2-\varepsilon_{fe}+i\Gamma_{fe}}\right.$$
$$\left.\left.-\frac{1}{\Omega_2-\varepsilon_{eg}+i\Gamma_{eg}}\right]\right\}. \quad (45)$$

The RPE signals from an anharmonic three level system are summarized in Table I, which gives for each resonance peak in the total RPE signal [Fig. 5(a)] all terms that contribute with their amplitude and dephasing rate (which in the frequency domain determines the line width).

Finally, when comparing the variation with t_{ba}, we see that while the ordinary RPE signal is a damped oscillation with frequency ε_{fg} and dephasing rate Γ_{fg}, the local-field contribution is a superposition of two oscillations with ε_{fg} and $2\varepsilon_{eg}$. In the homodyne-detected signal, where the square of the amplitude is measured, the former gives a single damped exponential with a dephasing rate $2\Gamma_{fg}$, while the local-field contributions should show a more complex pattern, where the beat frequency with a period corresponding to the anharmonicity, are clearly distinguishable. Such a behavior can be seen in Fig. 3, which shows the square of the amplitude of the two contributions to the total RPE polarization vs. t_{ba} for a fixed value of t_{cb}. (Note that this corresponds to a time-gated detection; in a homodyne experiment one would have to integrate over t_{cb}.) We see that the anharmonicity of $\Delta=20\ \mathrm{cm}^{-1}$ shows up in the oscillation period of $T=1.7$ ps and the dephasing of $\Gamma_{fg}=2\Gamma_{eg}=2\ \mathrm{cm}^{-1}$ corresponds to a dephasing time scale of $T_2/2=8$ ps with t_{ba}. As a function of t_{cb} the ordinary echo signal has a slower $\Gamma_{eg}=1\ \mathrm{cm}^{-1}$ damping, while the local-field contributions show a complicated behavior, with an initial rise time.

C. Two coupled three level systems

To simulate the complete RPE signal of two coupled anharmonic vibrations, we used the values found in photon echo experiments[47,48] for the symmetric and asymmetric CO stretches in rhodium(I) dicarbonylacetylacetonate (RDC).[46] The level scheme is shown in the inset of Fig. 7 and the transition energies are $\varepsilon_{e1,g}=2085\ \mathrm{cm}^{-1}$ and $\varepsilon_{e1,g}=2014\ \mathrm{cm}^{-1}$. The values of the anharmonic splittings are $\Delta_1=10.6\ \mathrm{cm}^{-1}$, $\Delta_2=12\ \mathrm{cm}^{-1}$, and $\Delta_3=25\ \mathrm{cm}^{-1}$ and the dipole moments are assumed to be $\mu_{e1,g}=\mu_{e2,g}$, $\mu_{f1,e1}=\mu_{f2,e2}=1.3\mu_{e1,g}$, $\mu_{f3,e1}=\mu_{f3,e2}=0.9\mu_{e1,g}$, and $\mu_{f1,e2}$

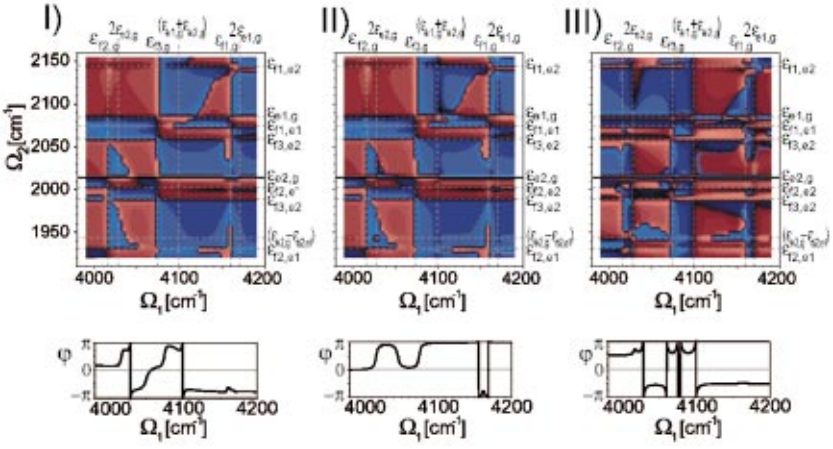

FIG. 8. (Color) The phase of the 2D-FT signals shown in Fig. 7. Lower row shows a slice for constant $\Omega_2=\varepsilon_{e2,g}$, see text for details.

μf1,e2$=\mu_{f2,e1}=-0.04\mu_{e1,g}$. The dephasing rate was set to $\Gamma_{e1,g}=\Gamma_{e2,g}=1\,\mathrm{cm}^{-1}$ and the double excited states were assumed to dephase with twice this rate $\Gamma_{fi,g}=2\Gamma_{ei,g}$, while population relaxation was neglected $\Gamma_{ei,ej}=\Gamma_{g,g}=0$.

Figure 7 shows the resulting 2D-FT RPE signal. Note that due to the anharmonicity, otherwise forbidden transitions contribute as well and give weak signals at $\Omega_2=\varepsilon_{f1,e2}$ and $\Omega_2=\varepsilon_{f2,e1}$, which are shown magnified by a factor of 20. In addition to the ordinary RPE resonances, we find new peaks at twice, and at the sum of the two single-exciton frequencies. Thus, instead of resonances only at $\Omega_1=\varepsilon_{f2,g},\varepsilon_{f3,g},\varepsilon_{f1,g}$ [as expected for the ordinary RPE (case I in Fig. 7)], we find six ''columns'' with peaks because the local-field resonances can also occur at all combinations of single exciton energies. Local-field effects thus show very distinct features in the RPE signal.

Note that the local field contributions [shown in Fig. 7 (III)] have their most pronounced peaks at resonances of $\Omega_1=2\varepsilon_{e1,g},2\varepsilon_{e2,g},(\varepsilon_{e1,g}+\varepsilon_{e2,g})$, but also make a contribution to the resonances of the ordinary RPE signal. Local-field effects also show a very different variation of phase as shown in Fig. 8, which displays the phase of the entire 2D spectrum, as well as a slice along the Ω_1 axis for a fixed value of $\Omega_2=\varepsilon_{e2,g}$.

VI. CONCLUSIONS

Comparison of the resonances of coupled systems and the local field-induced resonances found in a system of independent chromophores shows several fundamental differences. While interaction induced resonances contain information about the local microscopic environment,[5] the macroscopic local field-induced resonances simply show combinations of one-exciton resonances and do not yield additional microscopic information. When inhomogeneous broadening is included, we might get different information about the macroscopic sample than from linear spectroscopy, since the average of a product of correlation functions is different from the product of averages. For the heterodyne detected four wave mixing signal of a general aggregate built from interacting chromophores, we expect a complex pattern resulting from both short- and long-range effects, as demonstrated here for the reverse photon echo in several model systems. In addition to the two-exciton bands, we expect new local-field resonances, with a different dependence on concentration.

Local fields can also be viewed as a retardation effect which leads to breakdown of time ordering in an impulsive experiment. The third order response function in the time domain, which describes ideal impulsive experiments, has 8 terms. The corresponding frequency domain susceptibility includes 48 terms corresponding to all six permutations of the three fields.[1] The former has absolute control of time orders. The latter has no time control at all; see e.g., doubly resonant vibrationally enhanced IR-FWM.[49,50] As the pulses become longer, impulsive experiments start to assume a frequency domain character and realistic experiments will be intermediate and may contain more terms than in the impulsive case. Also in an ideal impulsive experiment the local fields that interact with the molecules are no longer impulsive and macroscopic many-body effects can have major influences on the signal.

Other types of collective resonances related to continuous manifolds of levels were predicted[6,51] Intermolecular resonances were observed in fifth order Raman.[15] Local-field effects in fifth order Raman of CS_2[26,52] were simulated recently.[53] High harmonic resonances have been observed in NMR.[30,31] In optical $\mathbf{k}_1+\mathbf{k}_2-\mathbf{k}_3$ signals these resonances have not yet been directly resolved. In studies on semiconductor quantum wells[21,22] a RPE signal was observed, decaying with twice the dephasing rate in a transient grating experiment. Since those experiments used homodyne detection, they could not observe the resonances at twice the optical resonance frequency. Recent experiments[23,24] on iodine vapor also revealed the RPE signal for negative time delays in a photon-echo setup. Again homodyne detection was used, but due to the special level structure in iodine, vibrational quantum beats are observed. A careful analysis of this signal as a function of t_{ba} should be able to reveal differences in the wave packet structure, which however, for a nearly harmonic system are very small and were not resolved. Further in Ref. 23 the focus was on a different three pulse scheme, where the time delay between the first and second pulse was varied (this was assumed to be zero here) and the time between the second and the third pulse (corresponding to our t_{ba}) was fixed. Heterodyne detected four wave mixing experiments[43] are necessary in order to observe the predicted high harmonic resonances in optical signals.

ACKNOWLEDGMENTS

The support of the National Institutes of Health (GM59230-01A2) and the National Science Foundation (CHE-9814061) is gratefully acknowledged. The stay of author A.T. at Rochester was funded by the Austrian Special Research Program F016 ''ADLIS'' (Austrian Science Foundation Vienna/Austria).

APPENDIX A: THE FOUR WAVE MIXING K_{RPE} SIGNAL

For the model aggregate described in Sec. III, the total signal [Eq. (27)] can be evaluated analytically and the final expressions for the individual terms in Eqs. (28) and (29) are given in the following. In this appendix we use the compact notation

$$\bar{\epsilon}_{ij}\equiv\varepsilon_{ij}-i\Gamma_{ij}, \tag{A1}$$

i.e., we include the dephasing in the site energies. (In the main text we showed the dephasing rates explicitly.)

Due to the breakdown of time ordering, we also need to take into account R_{II} (see Fig. 2) for one of the terms in Eq. (15). Three Liouville space pathways contribute to R_{II}:

$$R_{II}=i^3(R_4+R_5+R_6), \tag{A2}$$

$$R_4(t,\tau_3,\tau_2,\tau_1)=\Theta\sum_{e,e',g}\mu_{eg}\mu_{e'g}\mu_{e'g}\mu_{eg}\times\exp[-i\bar{\epsilon}_{eg}(t-\tau_3)]\times\exp[-i\bar{\epsilon}_{ee'}(\tau_3-\tau_2)]\times\exp[-i\bar{\epsilon}_{eg}(\tau_2-\tau_1)] \tag{A3}$$

$$R_5(t,\tau_3,\tau_2,\tau_1)=\Theta\sum_{e,e'}\mu_{eg}\mu_{ge}\mu_{e'g}\mu_{ge'}\times\exp[-i\bar{\epsilon}_{e'g}(t-\tau_3)]\times\exp[-i\bar{\epsilon}_{gg}(\tau_3-\tau_2)]\exp[-i\bar{\epsilon}_{eg}(\tau_2-\tau_1)] \tag{A4}$$

$$R_6(t,\tau_3,\tau_2,\tau_1)=\Theta\sum_{e,e'}\mu_{eg}\mu_{e'g}\mu_{fe}\mu_{e'f}\times\exp[-i\bar{\epsilon}_{fe'}(t-\tau_3)]\times\exp[-i\bar{\epsilon}_{ee'}(\tau_3-\tau_2)]\times\exp[-i\bar{\epsilon}_{eg}(\tau_2-\tau_1)] \tag{A5}$$

Using Eqs. (18), (A2), (17), and (23), the integrations in the expressions of Eqs. (28) and (29) can be performed and we easily find the expressions for the polarization corresponding to each of the contributions depicted in Fig. 1. In terms of the time intervals t_{cb} and t_{ba} they are given by

$$P^{(3)}_{OR}(t_{cb},t_{ba})=i^3\rho_0E_a^2E_b^*\sum_{e,e',f}\mu_{eg}\mu_{fe}\mu_{e'f}[\mu_{ge'}\exp[-i\bar{\epsilon}_{e'g}t_{cb}]-\mu_{e'g}\exp[-i\bar{\epsilon}_{fe'}t_{cb}]]\exp[-i\bar{\epsilon}_{fg}t_{ba}] \tag{A6}$$

$$P^{(3)}_{LF_I}(t_{cb},t_{ba})=i^3\frac{4\pi}{3}\rho_0^2E_a^2E_b^*\sum_{e,e',e'',f}|\mu_{e''g}|^2\mu_{eg}\mu_{fe}\mu_{e'f}\exp[-i\bar{\epsilon}_{fg}t_{ba}]\left[\mu_{ge'}\frac{\exp[-i(\bar{\epsilon}_{fg}-\bar{\epsilon}^*_{e''g})t_{cb}]-\exp[-i\bar{\epsilon}_{e'g}t_{cb}]}{\bar{\epsilon}^*_{e''g}+\bar{\epsilon}_{e'g}-\bar{\epsilon}_{fg}}-\mu_{e'g}\frac{\exp[-i(\bar{\epsilon}_{fg}-\bar{\epsilon}^*_{e''g})t_{cb}]-\exp[-i\bar{\epsilon}_{fe'}t_{cb}]}{\bar{\epsilon}^*_{e''g}+\bar{\epsilon}_{fe'}-\bar{\epsilon}_{fg}}\right] \tag{A7}$$

$$P^{(3)}_{LF_{II}}(t_{cb},t_{ba})=2i^3\frac{4\pi}{3}\rho_0^2E_a^2E_b^*\sum_{e,e',e'',f}|\mu_{e''g}|^2\mu_{eg}\mu_{fe}\mu_{e'f}[\exp[-i(\bar{\epsilon}_{eg}+\bar{\epsilon}_{e''g})t_{ba}]-\exp[-i\bar{\epsilon}_{fg}t_{ba}]]\frac{\mu_{ge'}\exp[-i\bar{\epsilon}_{e'g}t_{cb}]-\mu_{e'g}\exp[-i\bar{\epsilon}_{fe'}t_{cb}]}{\bar{\epsilon}_{fg}-\bar{\epsilon}_{eg}-\bar{\epsilon}_{e''g}} \tag{A8}$$

$$P^{(3)}_{LF_{III}}(t_{cb},t_{ba})=2i^3\frac{4\pi}{3}\rho_0^2E_a^2E_b^*\sum_{g,e,e',e'',f}|\mu_{e''g}|^2\mu_{eg}\exp[-i(\bar{\epsilon}_{eg}+\bar{\epsilon}_{e''g})t_{ba}]\times\left[\mu_{e'g}\mu_{ge'}\mu_{ge}\frac{\exp[-i(\bar{\epsilon}_{ee'}+\bar{\epsilon}_{e''g})t_{cb}]-\exp[-i\bar{\epsilon}_{eg}t_{cb}]}{\bar{\epsilon}_{eg}-\bar{\epsilon}_{ee'}-\bar{\epsilon}_{e''g}}+\mu_{ge}\mu_{e'g}\mu_{ge'}\frac{\exp[-i(\bar{\epsilon}_{e''g}+\bar{\epsilon}_{gg})t_{cb}]-\exp[-i\bar{\epsilon}_{e'g}t_{cb}]}{\bar{\epsilon}_{e'g}-\bar{\epsilon}_{gg}-\bar{\epsilon}_{e''g}}-\mu_{e'g}\mu_{fe}\mu_{e'f}\frac{\exp[(-i(\bar{\epsilon}_{ee'}+\bar{\epsilon}_{e''g})t_{cb}]-\exp[-i\bar{\epsilon}_{fe'}t_{cb}]}{\bar{\epsilon}_{fe'}-\bar{\epsilon}_{ee'}-\bar{\epsilon}_{e''g}}\right] \tag{A9}$$

$$P^{(3)}_{LF_{IV}}(t_{cb},t_{ba})=i^3\frac{4\pi}{3}\rho_0^2E_a^2E_b^*\sum_{e,e',e'',f}|\mu_{e''g}|^2\mu_{eg}\mu_{fe}\mu_{e'f}\exp[-i\bar{\epsilon}_{fg}t_{ba}]\left[\mu_{ge'}\frac{\exp[-i\bar{\epsilon}_{e'g}t_{cb}]-\exp[-i\bar{\epsilon}_{e''g}t_{cb}]}{\bar{\epsilon}_{e''g}-\bar{\epsilon}_{e'g}}-\mu_{e'g}\frac{\exp[-i\bar{\epsilon}_{fe'}t_{cb}]-\exp[-i\bar{\epsilon}_{e''g}t_{cb}]}{\bar{\epsilon}_{e''g}-\bar{\epsilon}_{fe'}}\right]. \tag{A10}$$

The corresponding 2D-frequency domain expressions can be evaluated easily using Eq. (31), resulting in

$$S_{OR}(\Omega_2,\Omega_1)=i^3\rho_0E_a^2E_b^*\sum_{e,e',f}\mu_{eg}\mu_{fe}\mu_{e'f}\frac{1}{\Omega_1-\bar{\epsilon}_{fg}}\left[\frac{\mu_{ge'}}{\Omega_2-\bar{\epsilon}_{e'g}}-\frac{\mu_{e'g}}{\Omega_2-\bar{\epsilon}_{fe'}}\right] \tag{A11}$$

$$S_{LF_I}(\Omega_2,\Omega_1)=i^3\frac{4\pi}{3}\rho_0^2E_a^2E_b^*\sum_{e,e',f}|\mu_{e''g}|^2\mu_{eg}\mu_{fe}\mu_{e'f}\frac{1}{\Omega_1-\bar{\epsilon}_{fg}}\left\{\frac{\mu_{ge'}}{\bar{\epsilon}^*_{e''g}+\bar{\epsilon}_{e'g}-\bar{\epsilon}_{fg}}\left[\frac{1}{\Omega_2-(\bar{\epsilon}_{fg}-\bar{\epsilon}^*_{e''g})}-\frac{1}{\Omega_2-\bar{\epsilon}_{e'g}}\right]\right.$$
$$\left.-\frac{\mu_{e'g}}{\bar{\epsilon}^*_{e''g}+\bar{\epsilon}_{fe'}-\bar{\epsilon}_{fg}}\left[\frac{1}{\Omega_2-(\bar{\epsilon}_{fg}-\bar{\epsilon}^*_{e''g})}-\frac{1}{\Omega_2-\bar{\epsilon}_{fe'}}\right]\right\} \tag{A12}$$

$$S_{LF_{II}}(\Omega_2,\Omega_1)=2i^3\frac{4\pi}{3}\rho_0^2E_a^2E_b^*\sum_{e,e',f}|\mu_{e''g}|^2\mu_{eg}\mu_{fe}\mu_{e'f}\left[\frac{1}{\Omega_1-(\bar{\epsilon}_{eg}+\bar{\epsilon}_{e''g})}-\frac{1}{\Omega_1-\bar{\epsilon}_{fg}}\right]\frac{1}{\bar{\epsilon}_{fg}-\bar{\epsilon}_{eg}-\bar{\epsilon}_{e''g}}$$
$$\times\left[\frac{\mu_{ge'}}{\Omega_2-\bar{\epsilon}_{e'g}}-\frac{\mu_{e'g}}{\Omega_2-\bar{\epsilon}_{fe'}}\right] \tag{A13}$$

$$S_{LF_{III}}(\Omega_2,\Omega_1)=2i^3\frac{4\pi}{3}\rho_0^2E_a^2E_b^*\sum_{e,e',f}|\mu_{e''g}|^2\mu_{eg}\frac{1}{\Omega_1-(\bar{\epsilon}_{eg}+\bar{\epsilon}_{e''g})}\left\{\frac{\mu_{e'g}\mu_{ge'}\mu_{ge}}{\bar{\epsilon}_{eg}-\bar{\epsilon}_{ee'}-\bar{\epsilon}_{e''g}}\left[\frac{1}{\Omega_2-(\bar{\epsilon}_{ee'}+\bar{\epsilon}_{e''g})}-\frac{1}{\Omega_2-\bar{\epsilon}_{eg}}\right]\right.$$
$$\left.+\frac{\mu_{ge}\mu_{e'g}\mu_{ge'}}{\bar{\epsilon}_{e'g}-\bar{\epsilon}_{gg}-\bar{\epsilon}_{e''g}}\left[\frac{1}{\Omega_2-(\bar{\epsilon}_{gg}+\bar{\epsilon}_{e''g})}-\frac{1}{\Omega_2-\bar{\epsilon}_{e'g}}\right]-\frac{\mu_{e'g}\mu_{fe}\mu_{e'f}}{\bar{\epsilon}_{fe'}-\bar{\epsilon}_{ee'}-\bar{\epsilon}_{e''g}}\left[\frac{1}{\Omega_2-(\bar{\epsilon}_{ee'}+\bar{\epsilon}_{e''g})}-\frac{1}{\Omega_2-\bar{\epsilon}_{fe'}}\right]\right\} \tag{A14}$$

$$S_{LF_{IV}}(\Omega_2,\Omega_1)=i^3\frac{4\pi}{3}\rho_0^2E_a^2E_b^*\sum_{e,e',f}|\mu_{e''g}|^2\mu_{eg}\mu_{fe}\mu_{e'f}\frac{1}{\Omega_1-\bar{\epsilon}_{fg}}\left\{\frac{\mu_{ge'}}{\bar{\epsilon}_{e''g}-\bar{\epsilon}_{e'g}}\left[\frac{1}{\Omega_2-\bar{\epsilon}_{e'g}}-\frac{1}{\Omega_2-\bar{\epsilon}_{e''g}}\right]\right.$$
$$\left.-\frac{\mu_{e'g}}{\bar{\epsilon}_{e''g}-\bar{\epsilon}_{fe'}}\left[\frac{1}{\Omega_2-\bar{\epsilon}_{fe'}}-\frac{1}{\Omega_2-\bar{\epsilon}_{e''g}}\right]\right\}. \tag{A15}$$

[1] S. Mukamel, *Principles of Nonlinear Optical Spectroscopy* (Oxford, New York, 1995).
[2] D. Bedeaux and N. Bloembergen, Physica (Amsterdam) **69**, 67 (1973).
[3] *Ultrafast Phenomena XII*, edited by T. Elsasser, S. Mukamel, M. M. Murnane, and N. F. Scherer (Springer-Verlag, Berlin, 2000).
[4] S. Mukamel and R. M. Hochstrasser, Special Issue on Multidimensional Spectroscopies, Chem. Phys. **266**, 2 (2001).
[5] S. Mukamel, Annu. Rev. Phys. Chem. **51**, 691 (2000).
[6] V. Chernyak, N. Wang, and S. Mukamel, Phys. Rep. **263**, 213 (1995).
[7] J. A. Leegwater and S. Mukamel, J. Chem. Phys. **101**, 7388 (1994).
[8] S. Mukamel, Z. Deng, and J. Grad, J. Opt. Soc. Am. B **5**, 804 (1988).
[9] H. A. Lorentz, *The Theory of Electrons* (Dover, New York, 1952).
[10] S. Mukamel, in *Molecular Nonlinear Optics*, edited by J. Zyss (Academic, New York, 1994).
[11] J. Knoester and S. Mukamel, Phys. Rev. A **39**, 1899 (1989); *ibid.* **41**, 3812 (1990).
[12] W. M. Zhang, V. Chernyak, and S. Mukamel, J. Chem. Phys. **110**, 5011 (1999).
[13] S. Woutersen, Y. Mu, G. Stock, and P. Hamm, Chem. Phys. **266**, 137 (2001).
[14] P. Hamm, M. Lim, W. F. DeGrado, and R. M. Hochstrasser, J. Chem. Phys. **112**, 1907 (2000).
[15] A. Tokmakoff, M. J. Lang, D. S. Larsen, G. R. Fleming, V. Chernyak, and S. Mukamel, Phys. Rev. Lett. **79**, 2702 (1997).
[16] *Ultrafast Infrared and Raman Spectroscopy*, edited by M. Fayer (Dekker Inc., New York, 1999).
[17] D. D. Dlott, Chem. Phys. **266**, 149 (2001).
[18] J. Stenger, D. Madsen, J. Dreyer, E. T. J. Nibbering, P. Hamm, and T. Elsaesser, J. Phys. Chem. A **105**, 2929 (2001).
[19] S. Mukamel and D. S. Chemla, Special Issue on Confined Excitations in Molecular and Semiconductor Nanostructures, Chem. Phys. **210**, 1 (1996).
[20] S. Wu, J. Appl. Phys. **73**, 8035 (2001).
[21] K. Leo, M. Wegener, J. Shah, D. S. Chemla, E. O. Göbel, T. C. Damen, S. Schmitt-Rink, and W. Schäfer, Phys. Rev. Lett. **65**, 1340 (1990).
[22] S. Schmitt-Rink, S. Mukamel, K. Leo, J. Shah, and D. S. Chemla, Phys. Rev. A **44**, 2124 (1991).
[23] V. Lozovoy, I. Pastirk, M. G. Comstock, and M. Dantus, Chem. Phys. **266**, 205 (2001).
[24] B. I. Grimberg, V. V. Lozovoy, M. Dantus, and S. Mukamel, J. Phys. Chem. A (in press), (2002).
[25] S. T. Cundiff, J. M. Shacklette, E. A. Gibson, in *Ultrafast Phenomena XII*, edited by T. Elsasser, S. Mukamel, M. M. Murnane, and N. F. Scherer (Springer, Berlin, 2000), pp. 344–346; S. T. Cundiff, J. M. Shacklette, and V. O. Lorenz, "Interaction Effects in Optically Dense Materials," SPIE 2001, preprint.
[26] D. A. Blank, L. J. Kaufman, and G. R. Fleming, J. Chem. Phys. **111**, 3105 (1999).
[27] L. J. Kaufman, J. Heo, G. R. Fleming, J. Sung, and M. Cho, Chem. Phys. **266**, 251 (2001).
[28] F. C. Spano and S. Mukamel, Phys. Rev. Lett. **66**, 1197 (1991).
[29] S. Mukamel and A. Tortschanoff, Chem. Phys. Lett. (submitted).
[30] J. Jeener, A. Vlassenbroek, and P. Broekaert, J. Chem. Phys. **103**, 1309 (1995).
[31] W. Richter and W. S. Warren, Concepts Magn. Reson. **12**, 396 (2000).
[32] Here we assume a single molecular species. This assumption simplifies the notation, without changing the relevant physics. For a mixture we have to replace $\rho_0\alpha(t)$ by $\Sigma_i\rho_0^i\alpha_i(t)$.
[33] J. C. Kirkwood and A. C. Albrecht, J. Raman Spectrosc. **31**, 107 (2000).
[34] T. Efthimiopoulos, M. E. Movsessian, M. Katharkis, and N. Merlemis, J. Appl. Phys. **80**, 639 (1996).
[35] I. Biaggio, Phys. Rev. Lett. **82**, 193 (1999).
[36] A. W. Albrecht, A. D. Hybl, S. M. Gallagher Faeder, and D. M. Jonas, J. Chem. Phys. **111**, 10934 (1999).
[37] C. Scheurer, A. Piryatinski, and S. Mukamel, J. Am. Chem. Soc. **123**, 3114 (2001).
[38] M. Dahlbom, T. Minami, V. Chernyak, T. Pullerits, V. Sundström, and S. Mukamel, J. Phys. Chem. B **104**, 3976 (2000).
[39] J. C. Kirkwood, C. Scheurer, V. Chernyak, and S. Mukamel, J. Chem. Phys. **114**, 2419 (2001).
[40] V. Chernyak, W. M. Zhang, and S. Mukamel, J. Chem. Phys. **109**, 9587 (1998).

[41] M. Cho, N. F. Scherer, G. R. Fleming, and S. Mukamel, J. Chem. Phys. **96**, 5618 (1992).
[42] N. F. Scherer, A. J. Ruggiero, M. Du, and G. R. Fleming, J. Chem. Phys. **93**, 856 (1990).
[43] W. P. de Boeij, M. S. Pshenichnikov, and D. A. Wiersma, Chem. Phys. Lett. **238**, 1 (1995).
[44] A. Tokmakoff, J. Phys. Chem. A **104**, 4247 (2000).
[45] S. M. Gallagher Faeder and D. M. Jonas, J. Phys. Chem. A **103**, 10489 (1999).
[46] M. Khalil and A. Tokmakoff, Chem. Phys. **206**, 213 (2001).
[47] O. Golonzka, M. Khalil, N. Demirdöven, and A. Tokmakoff, Phys. Rev. Lett. **86**, 2154 (2001).
[48] K. A. Merchant, D. E. Thompson, and M. D. Fayer, Phys. Rev. Lett. **86**, 3899 (2001).
[49] M. Bonn, C. Hess, J. H. Miners, T. F. Heinz, H. J. Bakker, and M. Cho, Phys. Rev. Lett. **86**, 1566 (2001).
[50] W. Zhao and J. C. Wright, Phys. Rev. Lett. **84**, 1411 (2000).
[51] T. V. Shahbazyan, I. E. Perakis, and M. E. Raikh, Phys. Rev. Lett. **84**, 5896 (2000).
[52] V. Astinov, K. J. Kubarych, C. J. Milne, and R. J. Dwayne Miller, Chem. Phys. Lett. **327**, 334 (2000).
[53] T. I. C. Jansen, J. G. Snijders, and K. Duppen, J. Chem. Phys. **113**, 307 (2000); *ibid.* **114**, 10910 (2001).